Spot activity of late-type stars: a study of II Pegasi and DI Piscium

Marjaana Lindborg

Report 10/2014
Department of Physics
University of Helsinki
ISSN 1799-3024

UNIVERSITY OF HELSINKI REPORT SERIES IN ASTRONOMY

No. 10

Spot activity of late-type stars: a study of II Pegasi and DI Piscium

Marjaana Lindborg

Academic dissertation

Department of Physics
Faculty of Science
University of Helsinki
Helsinki, Finland

To be presented, with the permission of the Faculty of Science of the University of Helsinki, for public criticism in Hall 5 of The Main Building at The City Center Campus on 12.12.2014, at 12 o'clock noon.

Helsinki 2014

Supervisors: Docent Maarit J. Mantere
Department of Information and Computer Science
Aalto University

Docent Thomas Hackman
Department of Physics
University of Helsinki

Pre-examiners: Prof. Axel Brandenburg
Nordita, KTH Royal Institute of Technology
& Department of Astronomy
Stockholm University

Dr. Katalin Oláh
Konkoly Observatory
Hungarian Academy of Sciences

Opponent: Dr. Pascal Petit
IRAP
University of Toulouse

Custos: Prof. Karri Muinonen
Department of Physics
University of Helsinki

ISSN 1799-3024 (printed version)
ISBN 978-952-10-8967-1 (printed version)
Helsinki 2014
Helsinki University Print (Unigrafia)

ISSN 1799-3032 (pdf version)
ISBN 978-952-10-8968-8 (pdf version)
ISSN-L 1799-3024
http://ethesis.helsinki.fi/
Helsinki 2014
Electronic Publications @ University of Helsinki (Helsingin yliopiston verkkojulkaisut)

Marjaana Lindborg: **Spot activity of late-type stars: a study of II Pegasi and DI Piscium**, University of Helsinki, 2014, 82 p.+appendices, University of Helsinki Report Series in Astronomy, No. 10, ISSN 1799-3024 (printed version), ISBN 978-952-10-8967-1 (printed version), ISSN 1799-3032 (pdf version), ISBN 978-952-10-8968-8 (pdf version), ISSN-L 1799-3024
Keywords: spot activity, magnetic activity, Doppler imaging, II Peg, DI Psc

Abstract

All stars that have outer convection zones show magnetic activity. This activity strengthens with angular velocity and depth of the convection zone. Cool starspots are believed to be caused by local magnetic field concentrations on the surfaces of stars. They show up as dark regions against a bright photosphere and are observable manifestations of the internal dynamo activity. Therefore the solar dynamo is not unique, only one example of a cyclic dynamo. This makes studies of magnetic activity in other stars important.

The convection zone is believed to be the source area of the solar dynamo. The distributed dynamo paradigm is relying on magnetic field generation throughout the convection zone, while the flux-transport paradigm is based on the Babcock-Leighton -effect near the surface in which the mean poloidal field is produced by the merging of twisted magnetic loops. Mean-field dynamo models can produce many observed features both of the solar cycle and some of the features seen in active rapid rotators, but it remains yet under debate which dynamo paradigm is correct. Especially in the case of the Sun, the kinematic mean-field models of different types can lead to a satisfactory reproduction of the solar cycle main properties. These two prevailing dynamo paradigms are briefly introduced in this thesis, as well as their current challenges.

Time-series of stellar photometric, spectroscopic and spectropolarimetric observations help us draw conclusions on the type of the dynamo modes in other stars than the Sun, and thus improve our understanding about the solar dynamo itself. Starspots also aid us to do precise measurements of stellar rotation and yield information on the nonuniformities of rotational properties. Differential rotation is one of the key parameters in the stellar dynamo models and together with turbulent convection it is responsible for the dynamo action. Methods to detect starspots, their surface locations and migration patterns and their link with the stellar dynamo are presented in this thesis. Doppler imaging is an indirect method to calculate the surface temperature map of a star, and is based on the fact that the presence of spots on the stellar surface cause observable changes in photospheric absorption lines. The Doppler imaging method is applied on two targets, II Peg and DI Psc. Both stars show temporal variations in their spot distributions.

For II Peg our time series covers both states of high and low activity. Furthermore we discover a drift of the active region. This drift is also confirmed from photometry, with the carrier fit analysis. The most natural explanation for it would be an azimuthal dynamo wave. DI Psc is a rapidly rotating single giant, which has an interestingly high lithium concentration. We examine the spot behaviour for a two years time-span, and retrieve changes in the activity, which could indicate a fast activity cycle of only a few years.

Acknowledgements

Foremost, I would like to express my gratitude to my supervisors Dr. Maarit Mantere and Dr. Thomas Hackman, who have been valuable mentors to me, always willing to answer all my questions and encouraging me to finish my work. Special thanks to Dr. Maarit Mantere for all the guidance in theoretical astrophysics and computing, and to Dr. Thomas Hackman for helping me to understand several fine details in observing and observational astronomy that no courses ever taught. I am also thankful to my pre-examiners prof. Axel Brandenburg and Dr. Katalin Olah for fruitful comments in order to improve my thesis.

For my friends at the University, we had a great gang! Thanks for sharing the fun of all those great undergraduate parties and game events as well as physics calculus group with me, that made studying sciences a lot less lonely than it could have been. Thinking of those amazing years in Kumpula Campus still puts a big grin on my face. Special thanks goes to Arto, without you I would have never come this far.

After graduation I had the possibility to spend an amazing year working as a student support astronomer at the Nordic Optical Telescope in La Palma, Spain. That year was a true turning point in my life and I am still grateful to the Notties and ING students, you were my family in La Palma and made my stay in La Isla Bonita unforgettable. Also special thanks to my friends outside academia, especially to my Heureka gang for all the discussions in arts, politics, environmental issues and sciences - let's take a one bottle of red more!

Minna, my "sis", sometimes the world kept us apart, but when we meet, it is like no time has gone since the last meeting. Thanks for all the years you have been here for me, always ready to listen to my problems and encouraging me to start new things in my life. Annu, thank you for being such a patient friend to me. You have been seeing all my struggles in science and sometimes in life, thank you for sharing my strongest as well as the weakest moments with me. And now I am so grateful I have the honour to belong to both your families.

Finally, to my parents, thank you for your support and love, and for never questioning my life choices. One of the best parental advice I have gotten from you is to follow my own heart, because no one else can follow it for me. Rontti, Viiru and Remu, my beloved furballs, I promise to give you now more cuddles. Hugo, I will never forget the sacrifices you made just to stay by my side. Let's dive together to the deep blue unknown - Amo-te.

List of publications

Paper I: M. Lindborg, M.J. Korpi, T. Hackman, I. Tuominen, I. Ilyin, and N. Piskunov, 2011, "Doppler images of the RS CVn binary II Pegasi during the years 1994-2002", Astronomy & Astrophysics, 526, A44

Paper II: T. Hackman, M.J. Mantere, **M. Lindborg**, I. Ilyin, O. Kochukhov, N. Piskunov, and I. Tuominen, 2012, "Doppler images of II Pegasi for 2004-2010", Astronomy & Astrophysics, 538, A126

Paper III: T. Hackman, M.J. Mantere, L. Jetsu, I. Ilyin, P. Kajatkari, O. Kochukhov, J. Lehtinen, **M. Lindborg**, N. Piskunov, and I. Tuominen, 2011, "Spot activity of II Peg", Astronomische Nachrichten, 332, 859

Paper IV: M. Lindborg, M.J. Mantere, N. Olspert, J. Pelt, T. Hackman, G.W. Henry, L. Jetsu, and K.G. Strassmeier, 2013, "Multiperiodicity, modulations and flip-flops in variable star light curves. II. Analysis of II Pegasus photometry during 1979-2010", Astronomy & Astrophysics, 559, A97

Paper V: M. Lindborg, T. Hackman, M.J. Mantere, H. Korhonen, I. Ilyin, O. Kochukhov, and N. Piskunov, 2014, "Doppler images of DI Psc during 2004-2006", Astronomy & Astrophysics, 562, A139

Contents

Chapter 1

Introduction

Magnetic fields play a crucial role in both theoretical and observational astrophysics. They influence everything, from the dynamics of interstellar matter in galaxies and its ability to form stars and the resulting magnetic activity phenomena, to the evolution of interstellar matter all the way to planetary magnetospheres providing shelter for life on our planet. Our closest star, the Sun, is no exception (Fig.1.1). The knowledge that the Sun is magnetically active has inspired studies of magnetic activity on other stars. The links between stellar activity and evolution is demonstrated in Fig.1.2. This figure shows how internal structure, kinematics and dynamics are affected by dynamo action. We still do not know in detail what kind of dynamo mechanism causes the complex magnetic cycle of the Sun, and all observed magnetic phenomena, such as sunspots, flares, prominences and coronal mass ejections (CMEs). Studying the solar-stellar connection has a key role in developing our understanding of the theory for hydromagnetic dynamos and under which conditions they can be excited, and how the magnetic field is regenerated and sustained against diffusive effects.

Astronomers have been attracted by solar activity long before knowing the magnetic connection of the Sun and the Earth by observing aurorae both in the Northern and Southern Hemispheres. Also studies based on visual drawings of sunspots were done a long time before modern instruments, e.g. high-resolution spectrographs, were developed to enable more direct observational data. The first records of sunspot observations date back to Chinese astronomers more than 2000 years ago (Kopf, 2009), but only in 1908 Hale proved, that sunspots are associated with strong magnetic fields (Hale, 1908). According to a widely accepted theory sunspots are caused by magnetic flux tubes forming loops and rising from the convection zone. Colder regions form due to the slower plasma movements along the strong radial magnetic field lines penetrating the surface. The time variations in the sunspot activity are explained with an oscillatory dynamo mode exhibiting a latitudinally migrating dynamo wave.

It is nowadays known that most of the solar activity phenomena are a consequence of the magnetic field of the Sun. Magnetism of the Sun occurs on all scales. The

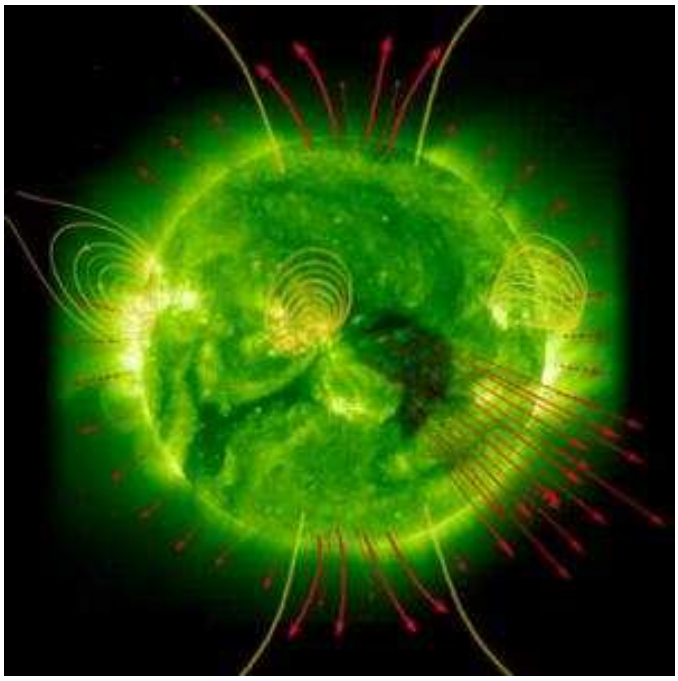

Figure 1.1: The Sun's atmosphere is threaded with magnetic fields. (Image Credit: September 18, 2003 image from the SOHO Extreme Ultraviolet Imaging Telescope. ESA/NASA)

smallest magnetic field flux tubes are at the limit of the spatial resolution of the observations, and the largest mean-field components may cover an entire hemisphere. All magnetic activity in the Sun is produced by the solar dynamo. The physics behind the stellar magnetic activity is mostly based on the studies of the Sun, especially its cool spots, flares, and other easily observable phenomena. Stars appear to us as distant pointsources, so it is impossible to directly observe spots of the same size as in the Sun.

Dynamo models can be used to study magnetic activity in other stars, using a model reproducing the solar magnetic cycle as a starting point, and attempting to extend it to parameter regimes describing some other stars. This can be thought to represent the theoretical side of the studies related to the solar-stellar connection (see Chapter 3). The most suitable objects for observational studies of the solar-stellar connection are rapidly rotating late-type stars that may have huge magnetic spots that can cover even half of the visible hemisphere (e.g. Strassmeier, 1999). As these spots move accross the stellar surface due to star's rotation, their rotation causes significant changes in photospheric absorption lines and photometric magnitudes. That makes them attractive objects for magnetic activity studies. Time series analysis of photometry, Doppler imaging (DI), and Zeeman Doppler imaging (ZDI) are commonly used

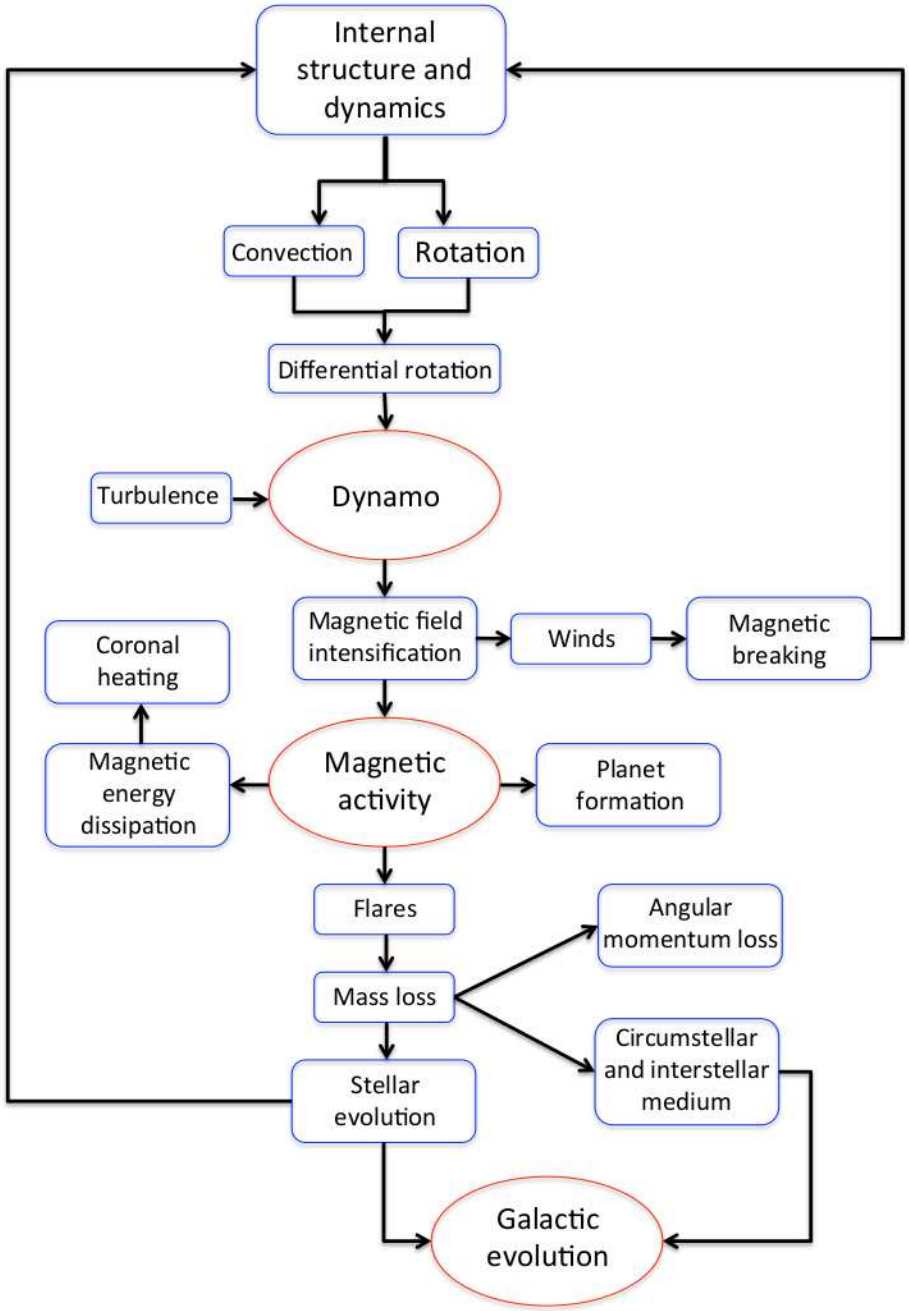

Figure 1.2: A sketch of the connection between internal structure, kinematics, dynamics and dynamo action in stars, influencing planet formation and galactic evolution. Figure adapted from Rodonò (2000).

methods to analyze spots in magnetically active stars. The rotation period, light-curve amplitude and long-term luminosity variations of the star can be determined with time series analysis, and the results can be used e.g. to determine possible active longitudes of the stars. One example of using photometry is the method called carrier fit (CF) analysis (Pelt *et al.*, 2011), which can be helpful in detecting e.g. drifts of spots and phase jumps. The CF method is suitable for analyzing time series in which a fast clocking frequency, such as the rotation of the star, is modulated with a slower process such as changes in the spot activity.

Photometric time series analysis cannot provide accurate two-dimensional images of the stellar surface, so DI and ZDI are needed to study the surface structure of stars. The main idea in these methods is to use rotationally broadened spectral line profiles of fast rotating active stars to map their surface structures (Vogt *et al.*, 1987). When the star rotates rapidly, so that the rotational broadening of a line profile is significantly larger than the local line profile of a single element on the stellar surface, cool starspots can be seen as bumps in the profile. These move accross the observed spectral line profile due to the Doppler effect. A surface map of the star can be retrieved by solving the inversion problem of a time series of the line profiles.

The knowledge that we have obtained by observing the Sun and other stars has allowed us to obtain a deeper understanding of the evolution of stellar magnetic activity. Many rapidly rotating, magnetically active stars can be seen as analogues of the young Sun, which makes them important to study. We still lack the fine details of the exact nature of the solar dynamo, e.g. in which layer the solar dynamo is operating and how to produce the irregular part of the observed solar cycle variations, like the variable strengths and lengths of the sunspot cycles. Furthermore it is still uncertain to what extent starspots are equivalent to sunspots. Thus in the future more DI and ZDI maps are needed, as well as more sophisticated dynamo models for varying types of late-type stars across the HR-diagram to reproduce the observed phenomena.

In this thesis, DI and the CF analysis are used to study starspots on two interesting magnetically active stars, the RS CVn star II Pegasi (hereafter II Peg), and the K-type lithium-rich giant DI Piscium (hereafter DI Psc). II Peg is one of the most frequently observed RS CVn binaries. The long photometric, spectroscopic and spectropolarimetric time series obtained are making it suitable for testing different dynamo models, and even determining possible dynamo waves, or differential rotation. DI Psc is a less known evolved giant, whose high lithium abundance compared to normal stars where lithium is destroyed soon after formation, and fast rotation make it an interesting target for Doppler imaging and activity cycle studies.

The aim of this thesis is to provide an observational view to the magnetic activity of rapidly rotating late-type stars, first of all summarizing what is known from

the previous studies of these objects, and then presenting case studies of the two chosen targets. Our approach is to interpret the observations from the point-of-view of dynamo theory. Therefore, a concise summary of dynamo theory and its main challenges are also presented. In this context a particular emphasis is on detecting evolution patterns from the spectral and photometric observations.

Chapter 2

Observational view of stellar magnetic activity

2.1 Solar magnetism and cycle

Since early days astronomers have been attracted by phenomena related to solar activity. Nowadays it is known that the activity is a consequence of the magnetic fields of the Sun. The knowledge of the physics behind the stellar magnetic activity is mostly based on the studies of the Sun, the only star of which we can have direct observations. All the observed magnetic activity in the Sun occurs in the solar atmosphere, which consists of four main regions: the photosphere, the chromosphere, the corona and the heliosphere. The sunspots occur in the photosphere, i.e. the Sun's visible surface. Prominences and flares are observed in the layer above, the chromosphere. The hot corona is the outer layer of the solar atmosphere, from where solar winds are blown out from the Sun to the heliosphere. The origin of magnetic activity of the Sun is the solar dynamo, which is a mechanism transforming the kinetic energy of the fluid motions into magnetic form. The most visible proofs of dynamo action are the sunspots seen on the solar surface (see Fig. 2.1) and their 11 year cycle, found by Schwabe (1844).

Solar activity studies were based on sunspots a long time before modern instrumentation was available. Sunspots have regularly been observed and mapped over 400 years, since the early 17th century, when Galileo Galilei, among others, first turned his telescope to the Sun. From those observations he drew the conclusion that these spots are surface features that move as the Sun rotates. In 1908, Hale proved that sunspots are associated with strong magnetic fields (Hale, 1908). Sunspots are cooler and darker regions on the photosphere caused by magnetic flux tubes rising from the convection zone.

The sunspot activity has a cyclic behaviour, which follows certain rules. The sunspot number follows the Schwabe cycle (Schwabe, 1844) with an average period of

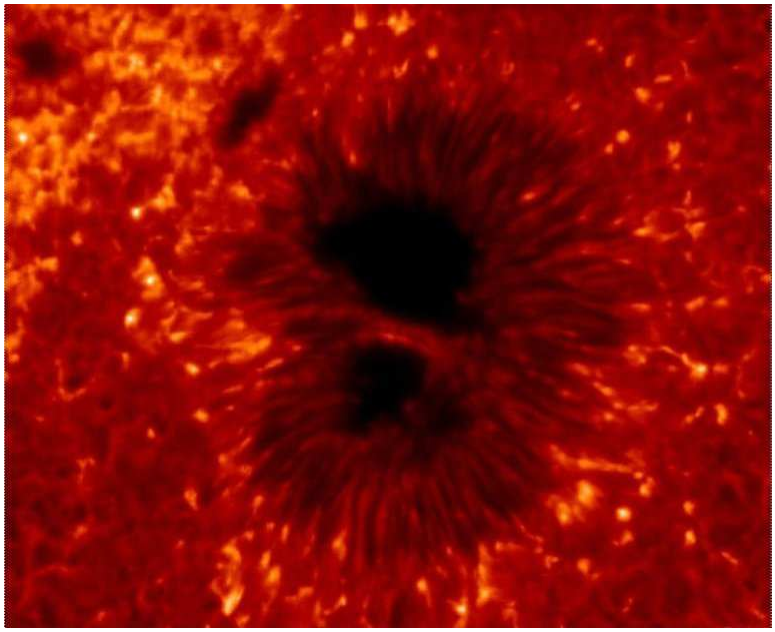

Figure 2.1: An Earth-sized sunspot seen by Hinode (Image Credit: Hinode NAOJ/NASA).

11 years. This is a consequence of the total 22-year magnetic Hale cycle, with a change of polarities around each 11 years (Hale *et al.*, 1919). Sunspots are often observed in bipolar groups. According to the Hale-Nicholson polarity rule the magnetic polarities of the leading and trailing spots are opposite, and also opposite in both hemispheres. The predominant sunspot polarities reverse after the sunspot minimum, i.e. approx. each 11 years (Hale *et al.*, 1919). The number and area of sunspots vary in time. Also the latitude of the spots on the solar disk is variable over time. The axes of sunspot pairs are tilted with respect to the solar equator and the leading spot is closer to the equator (Hale *et al.*, 1919). This is called Joy's law. In the beginning of the cycle, sunspots predominantly form at two belt-like areas centered at latitudes $\pm 27^\circ$. When the cycle goes on, the midpoints of the belts migrate toward the equator to about $\pm 8^\circ$ (Spörer's law), and the latitudinal occurrence of spots over time forms the famous butterfly diagram (Fig. 2.3). The width of the belts is about 36° at sunspot maximum. The ending of the old spot cycle and starting of the new one does not occur at a certain point in time. The cycles can overlap during a few years around the sunspot minimum.

Earlier sunspot cycles can be hindcasted back in time indirectly for example from aurora observations and cosmogenic radio-nucleides (e.g. Solanki *et al.*, 2004). From this type of data, it is evident that there are also other longer term variations in the sunspot amplitudes and lengths, in particular the Grand Minima. The best known

case is the Maunder Minimum, a 70 year period of very few sunspots in approx. 1645-1715, which was the first one seen in the sunspot data. The last five to six cycles are referred to as the Modern Maximum.

The Sun's nonaxisymmetric mode is weak, below 10% from the total energy integrated over the time (Usoskin *et al.*, 2005). When the spot cycle reaches minimum, the non-axisymmetry degree increases (Pipin *et al.*, 2014). Sunspots are associated with active regions where other magnetic activity also occur. Prominences are rising flux-tubes, seen as loops of plasma joining the poles of bipolar magnetic regions, and can be observed in the solar chromosphere. Prominences can be divided into two categories, the quiescent and the active ones. The quiescent prominences are long-lived whereas active ones are short-lived. Like sunspots, prominences appear more often near the solar maximum. Solar flares are explosive events that release energy in various forms, such as accelerated particles. Chromospheric flares are the easiest to observe. Their brightness increases for several minutes, followed by a slow dimming phase. Larger flares often appear after a sudden disappearance of a filament.

Another observed phenomenon on the Sun is the longitudinal clustering of spots, flares and other magnetic activity to areas that can rotate at different speeds than the surface of the Sun. These activity nests can continuously show up over longer timescales, up to several years, with an average lifetime of roughly 10-15 Carrington rotations (Pelt *et al.*, 2010). Activity nests that occur near the equator rotate faster than the high-latitude ones indicating that the differential rotation influences their rotation.

2.2 Solar rotation profile and meridional circulation

The Sun rotates around its axis in about 30 days, and this rotation was first detected from sunspot observations in the 17th century. Later on Carrington (1863) measured the solar differential rotation from spots and nowadays the formula $A + B\sin^2\theta + C\sin^4\theta$ is used to express the solar differential rotation, where the poles rotate slower than the equator (Beck, 2000). In this formula, A ≈ 2.97 μ rad s^{-1} per day, is the equatorial rotation rate, B ≈ -0.48 μ rad s^{-1} per day and C ≈ -0.36 μ rad s^{-1} per day set the differential rotation rate and θ is the solar latitude (Snodgrass and Ulrich, 1990).

The angular velocity Ω in the Sun is in fact a function of both the stellar latitude and depth in the convection zone. Helioseismology has opened a new era for rotation profile studies, and nowadays we know quite well the internal rotation of the Sun, shown in Fig. 2.4. From this figure we can see that Ω has a positive radial gradient at low latitudes and a negative one at latitudes above 40°. The strongest shear is located in the region at the bottom of the convection zone, or just below it. In this

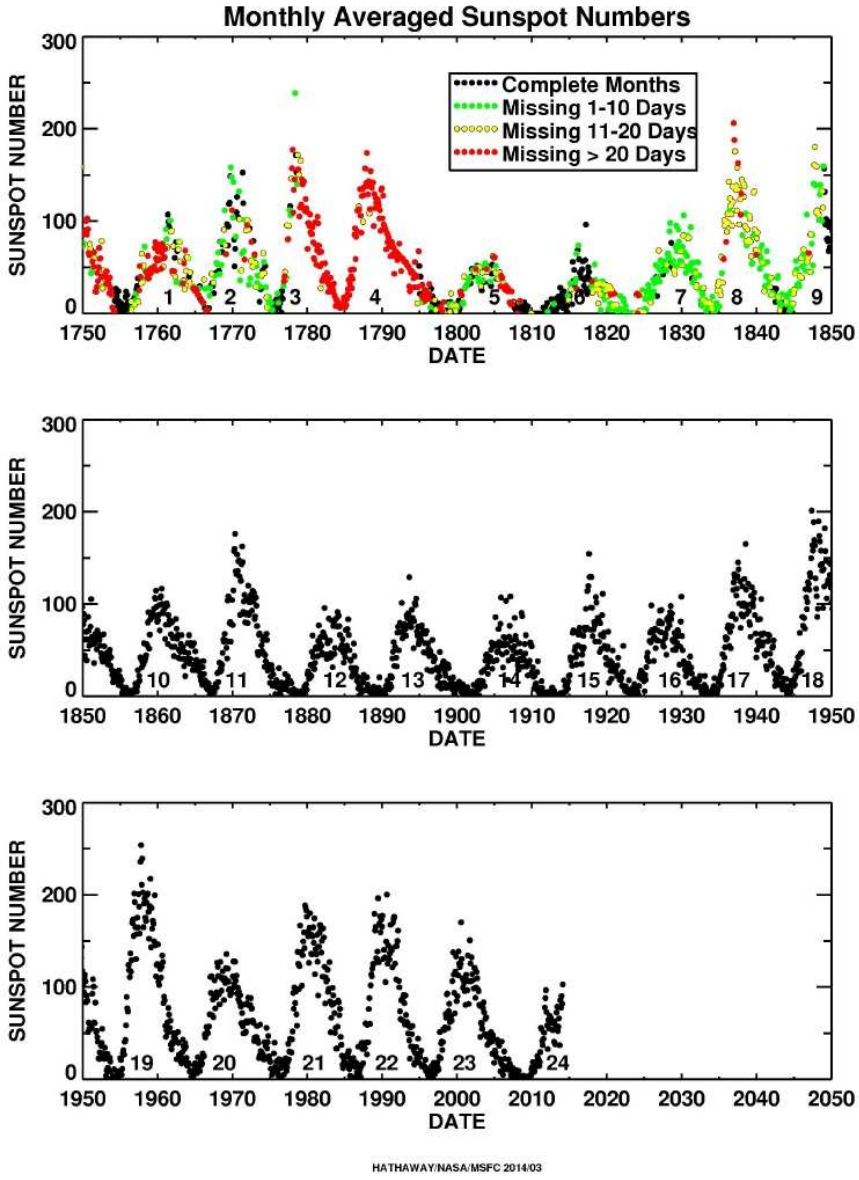

Figure 2.2: The varying lengths and amplitudes of sunspot cycles (Image Credit: D.H. Hathaway, NASA).

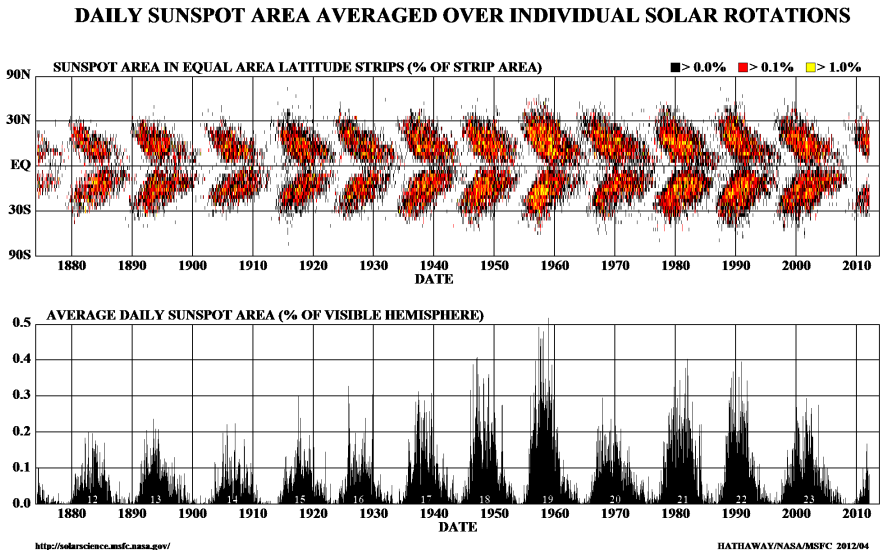

Figure 2.3: Upper panel: The latitudinal occurrence of sunspots over time with relative spot size ("butterfly diagram"). Lower panel: The average daily sunspot area. (Image Credit: D.H. Hathaway, NASA)

region, called the tachocline, the rotatation rate changes from differential rotation in the convection zone to nearly solid-body rotation in the interior. Already the early helioseismic inversions made by Duvall *et al.* (1984) showed angular velocities close to the surface of the Sun that were faster than the photospheric plasma determined from Doppler shifts. With more recent helioseismic inversions it became clear that there is a sharp shear layer located near the surface where the local rotation rate decreases outwards. Both shear layers might play an important role for dynamos (e.g. Brandenburg, 2005).

Differential rotation together with turbulent convection is responsible for the magnetic field generation in the Sun (Chapter 3). The change from the rigid rotation of the core to the latitudinally and radially changing rotation in the convection zone is explained by the different angular momentum transport mechanisms. Due to the long diffusion timescale in the radiative core the solid body rotation can exist because of a weak poloidal remnant magnetic field (Kitchatinov and Rüdiger, 2006) or weak turbulence created and driven by the magnetorotational instability (Arlt *et al.*, 2003; Kitchatinov and Rüdiger, 2006). Even weak turbulence could smoothen the gradients of Ω. The short diffusion time scale in the convection zone, however, suggests that there is a constant process that re-generates differential rotation.

The mean-field theory of stellar rotation (e.g. Rüdiger, 1989, and references therein) describes angular momentum transport in the turbulent and stratified con-

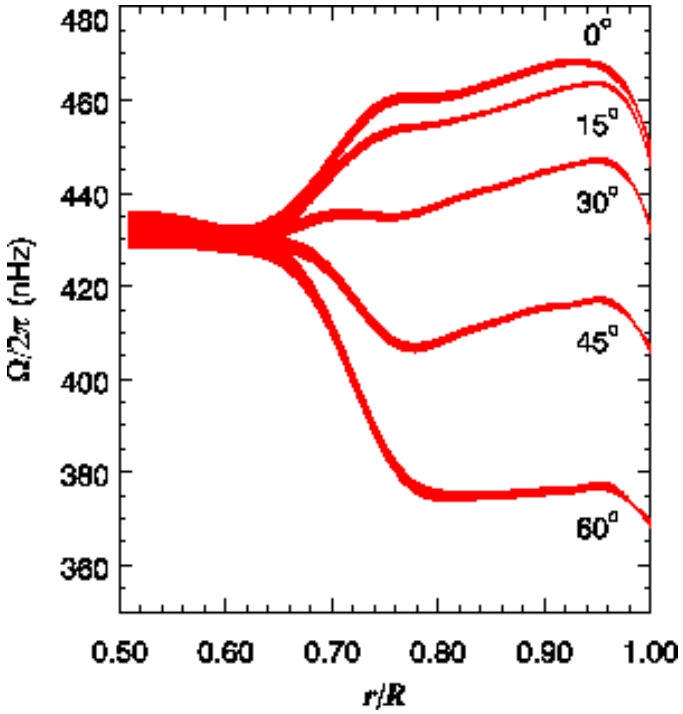

Figure 2.4: The internal rotation of the Sun obtained from helioseismology. The time-averaged rotation rates are plotted as a function of radius at different latitudes in the Sun. The tachocline, a region where the rotatation rate changes from differential rotation in the convection zone to nearly solid-body rotation in the interior, near the base of the convection zone, is determined to be at radius 0.71 R. (Image Credit: NSF's National Solar Observatory)

vection zone, anisotropized due to the presence of rotation. In such a system, turbulent Reynolds stresses provide angular momentum transport and heat fluxes. The generated rotation profile is further re-shaped with other effects such as meridional circulation and the baroclinic effect caused by latitudinal entropy variations (e.g. Warnecke *et al.*, 2013, and references therein). Fig. 2.5 presents a sketch of the meridional flow pattern and its amplitude in the solar convection zone. Recently, more accurate helioseismic measurements of the flow structures and have been done by Zhao *et al.* (2013) who found a double-cell meridional circulation profile with an equatorward flow shallower than previously thought. This is also consistent with direct numerical simulations (DNS, e.g. Miesch *et al.*, 2006, 2011; Käpylä *et al.*, 2012). These results are suggestive of a need to revise the simple sketch of Fig. 2.5, and consequently any dynamo model including a single-cell conveyor belt.

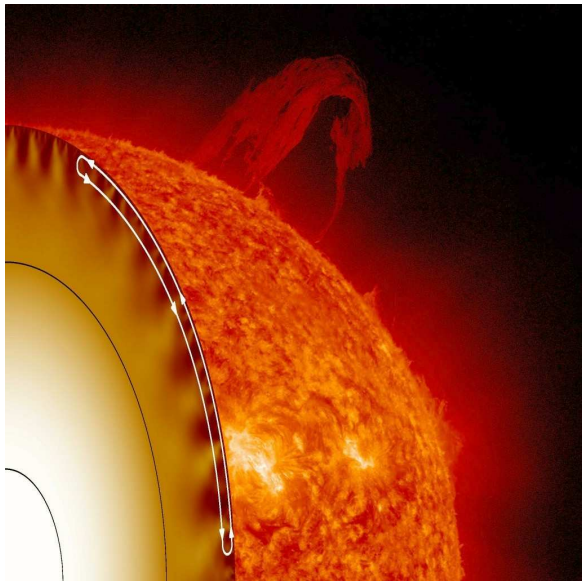

Figure 2.5: Meridional circulation in the Sun. At the surface this flow is 20 m/s, but the return flow toward the equator inside the Sun where the density is much higher must be much slower still - 1 to 2 m/s. This slow return flow would carry matter from the mid-latitudes to the equator in about 11 years (Image Credit: NASA).

2.3 From the Sun to other stars

All cool stars, either fully convective or with convective envelopes, like the Sun, most likely have spots on their surfaces (Strassmeier, 2009). Stars with outer convective zones have magnetic fields that strengthen in respect to angular velocity growth and decreasing Rossby number

$$Ro = \frac{P_{\rm rot}}{\tau_{\rm conv}}, \tag{2.1}$$

where $P_{\rm rot}$ is the rotation period and $\tau_{\rm conv}$ is the convective turnover time (Hall, 1991). According to this, therefore, rapidly rotating stars are more active than slow rotators, of the same spectral class. Instead of the Rossby number, the Coriolis number $\mathrm{Co} = 4\pi \mathrm{Ro}^{-1}$ is often used.

Cyclic variations have been observed mainly in stars that have B-V colors in the range 0.57 and 1.37, and spectral types of G0-K7 (Brandenburg and Subramanian, 2005; Baliunas *et al.*, 1995), but also some F-stars (Mathur *et al.*, 2014). Solar-stellar connection is a name for a research field investigating similarities and differences between solar and stellar activity. Very often an analogy is made between the properties of starspots vs. sunspots, assuming that they are formed in the process of very strong magnetic fields inhibiting convection in the surface regions of stars. There are, however, differences between observed starspots and sunspots. The indirectly observed spots in other stars are significantly larger than sunspots, and for the Sun the maxi-

mum luminosity is detected when the Sun is in spot maximum. In contrast, rapidly rotating active stars with large spots have a lower mean brightness when the spot activity increases, because the light curve is dominated by the effect from large spots (e.g. Radick *et al.*, 1990). However, while the luminosity change of the Sun is detected directly, the same is not true for stars, because in stars only small parts of the spectrum can be observed through filters, so the direct comparison can potentially be misleading. Magnetic breaking will slow down the rotation of a single star, eventually reducing the magnetic activity. Some theoretical models have been made to predict how rotation changes with mass and age (e.g. Barnes and Collier Cameron, 2001).

Unlike in the Sun, spots on rapidly rotating stars often appear on higher latitudes, even covering the rotation poles. This can be an effect of the larger Coriolis force deflecting rising magnetic flux tubes towards higher latitudes. In active stars the nonaxisymmetric component is stronger and active longitudes may rotate with a constant angular velocity, despite the surface differential rotation. Furthermore, the spot activity may concentrate on two permanent active longitudes, which are 180° apart from each other. One active longitude may dominate for a few years, and then the other active longitude becomes more active. This phenomenon was labelled as the flip-flop phenomenon and was first found in the single active giant FK Comae Berenices (Jetsu *et al.*, 1993). The phenomenon has been reported also in a few other stars, e.g., II Peg, σ Gem, EI Eri and HR 7275 (e.g. Berdyugina and Tuominen, 1998). The recent results on phase behaviour of stellar spots, however, imply that the flip-flops do not occur strictly periodically (e.g. Lindborg *et al.*, 2011). The connection of the flip-flop phenomenon to stellar cycles remain, therefore, unclear.

Stellar cycles can be detected by observations of Ca II H&K line fluxes and the mean stellar brightness variations. The mean brightness describes the spot coverage of active stars. The HK project at the Mount Wilson observatory has been one of the most succesful projects in stellar cycle detection (Wilson, 1978). Wilson's landmark paper (Wilson, 1978) showed the records of 91 stars, many with cyclic variations, and later on thousands of main sequence stars and giants were observed and analyzed. Many of these stars showed periodic behaviour (e.g. Lockwood *et al.*, 2007) and Baliunas and Jastrow (1990) concluded that some solar-type stars appeared to be in states resembling the solar grand minima.

Stellar spot cycles are naturally less well known than the one in the Sun. Some stars have multiple cycle periods, that suggest the same star has multiple dynamo modes. Some very active stars do not show any cyclic activity during the time of the observations. Most well-defined stellar cycles have periods between 5-15 years. The upper limit is, naturally, biased by the limited length of long-term studies. Cycles longer than 30 years would merely appear as a rise or a fall of stellar activity unless

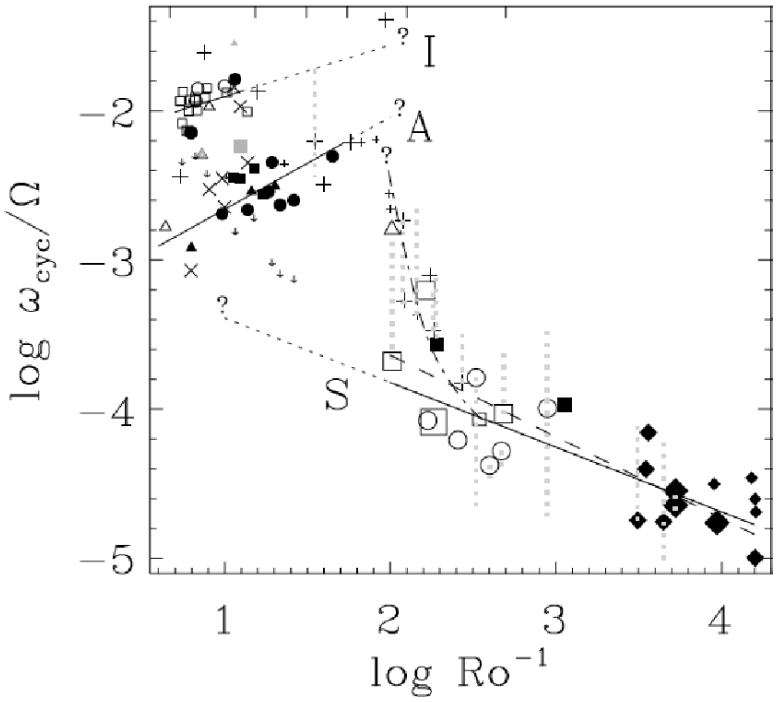

Figure 2.6: In a $\log \frac{\omega_{\rm cyc}}{\Omega}$ vs. $\log \mathrm{Ro}^{-1}$ diagramme late-type stars tend to group around three branches: inactive (I), active (A) and superactive (S). The symbols refer to different types of stars and the dash-dotted curve depicts a possible transition between the A and S branches. More details can be found in Saar and Brandenburg (1999). ©AAS. Reproduced with permission.

being in the middle of a maximum or minimum. As long as the time-limited data does not allow for long cycles to be repeated, these cycles may more likely reflect time scales of changes rather than periodicities (Oláh and Strassmeier, 2002; Oláh *et al.*, 2009). Saar and Brandenburg (1999) examined the dependence of the rotational-to-magnetic cycle period on the inverse Rossby number $\mathrm{Ro}^{-1} \equiv \tau_{\rm conv}/P_{\rm rot}$, describing the influence of rotation on the convective turbulence (with turnover time $\tau_{\rm conv}$) within the stellar convection zones in a large stellar sample of late-type stars at different evolutionary stages. Fig. 2.6 shows three different branches of stars: inactive, active and superactive. Stars of spectral type G–K are observed to show a large scatter in their rotational-to-magnetic cycle period: some fall on the sharp transition region in between the active and superactive branches, on which the magnetic cycle lengths strongly increse with respect to the rotation period, with $P_{\rm cyc}/P_{\rm rot}$ reaching values of one thousand or more. Some objects, however, also fall on the active branch with $P_{\rm cyc}/P_{\rm rot}$ of an order of magnitude smaller. A couple of RS Cvn binaries can also be seen in the inactive branch (Fig. 2.6). These stars can thus have cycles as long as 20 years, if they are in the transitory region, while on the active branch the cycle lengths would be on the order of a few years.

Because the activity has a dynamo origin, and dynamos are sensitive to rotation and its non-uniformities, there is a correlation between cycles, rotation and spectral classes of stars. With longer time series (>25 yr) of Ca II data and $P_{\rm cyc}$, it is reasonable to seek for correlations between $P_{\rm cyc}$ and other stellar properties. Brandenburg *et al.* (1998) studied those correlations and found out that the data suggest that the α-parameter (see Chapter 3) increases with magnetic field strength, contrary to the conventional idea of α-quenching. Stars seem to evolve with

$$\frac{\omega_{\rm cyc}}{\mathbf{\Omega}} \propto t^{-0.35}, \tag{2.2}$$

until the age t=2−3 Gyr, roughly at the Vaughan-Preston gap (Vaughan and Preston, 1980), where a sharp transition occurs, in which $\omega_{\rm cyc}/\mathbf{\Omega}$ increases by a factor of 6. The young, high-activity stars exhibit predominantly irregular cycles, while older, Sun-like stars have more well-defined cycles.

Stars with large spots open a simple way to study rotation. When the star rotates, the spots move accross the stellar disk. This dominates the total brightness of the star, thus giving a rotation period without knowing the inclination of the rotation axis. Rotation period measurements also enable estimating the differential surface rotation of spotted stars (e.g. Hall, 1972; Baliunas *et al.*, 1985), when the latitudinal location of a spot is known and the spots appear at different latitudes. When the latitude value is not known, we can still estimate the magnitude of the differential rotation but the latitudes cannot be safely determined from the one dimensional datasets.

In a recent study of $\sim$ 20 000 stars using the Kepler telescope, Reinhold *et al.* (2013) concluded that the absolute shear $\Delta\Omega = \Omega_{\rm eq} - \Omega_{\rm pole}$ showed a weak dependence on rotation period, while the relative shear $k = \frac{\Delta\Omega}{\Omega}$ increased with longer periods. This is consistent with previous results that

$$\frac{\Delta\Omega}{\Omega} \propto \Omega^{-n}. \tag{2.3}$$

n being positive it defines the decay of the relative differential rotation (e.g. Kitchatinov and Rüdiger, 1999) with the basic rotation. Observed values of n usually range between 0.3 (Donahue *et al.*, 1996) and 0.85 (Hall, 1991).

Chapter 3

Theories of stellar magnetism

This Chapter introduces the basis of dynamo theory, the two prevailing paradigms, namely the distributed and flux-transport dynamo models, and discusses their applicability to active late-type stars from an observational viewpoint.

3.1 Plasma state

In stars, matter is partly or fully ionized and carries electrical currents that produce magnetic fields. Matter of this kind is called plasma. The word plasma was first used by Langmuir in 1928 to define the ionized regions in gas discharges (Boyd and Sanderson, 2003), and has later been generalized to describe any state of matter forming a quasi-neutral ionized gas containing enough free charges to make electromagnetic effects important for its physical behaviour. Plasma is often called the fourth state of matter and is estimated to constitute a large portion of the visible baryonic universe.

In the interiors of the Sun and most stars, the collisional mean-free path of microscopic particles is a lot shorter than competing plasma length scales, fluid motions are non-relativistic, the plasma maintains a state of charge neutrality and is non-degenerate, which means that Ohm's law holds in these conditions. In order to exactly determine the magnetic fields that the charged particles create, one should know the position and velocity of every particle at all times. Following the motions of the charges in the fields they generate is possible only in simple cases. The dynamics of plasma interactions e.g., in a stellar convective flow are complex and beyond analytical techniques and exact numerical modeling.

Fortunately there is a more simple description of the plasma that is often accurate enough. Instead of specifying the plasma in terms of each of its particles, a macroscopic description of the plasma behaviour can be used, as in a fluid model. The fluid description of plasma refers to any simplified plasma treatment, where the quantities are averaged and smoothed over velocity space (see Subsection 3.2). In MHD a plasma is regarded as a fluid which is a very good conductor of electricity.

Depending on circumstances, this fluid description may be a one-fluid, a two-fluid, or a many-fluid approach. In the fluid approximation the plasma is treated as continuous matter, and in the one-fluid approximation the particles having different charges behave the same as the particles with same charges, because their Debye length, characterizing the spatial scale over which mobile charge carriers screen out electric fields, is tiny compared to the size of the fluid element (Boyd and Sanderson, 2003). Unlike neutral fluids, plasmas respond to electric and magnetic fields. Moving charged particles are influenced by the electromagnetic field via the Lorentz force, which cannot be neglected from the momentum equation of the gas. Since the volume elements of the plasma remain charge-neutral, large-scale electric fields do not exist, but currents flowing through the plasma can give rise to large-scale magnetic fields. MHD treats the plasma as a fluid governed by Maxwell's equations combined with the Navier-Stokes equations of fluid dynamics.

3.2 Basics of magnetohydrodynamics

Magnetohydrodynamics (MHD) is a study of the interaction of the magnetic field and the plasma that is treated like a fluid. In MHD the Maxwell's equations are

$$\nabla \cdot \mathbf{E} = \frac{1}{\epsilon_0}\rho_q \tag{3.1}$$

$$\nabla \cdot \mathbf{B} = 0 \tag{3.2}$$

$$\nabla \times \mathbf{E} = -\frac{\partial \mathbf{B}}{\partial t} \tag{3.3}$$

$$\nabla \times \mathbf{B} = \mu_0 \mathbf{j}, \tag{3.4}$$

where $\mathbf{E}$ is the electric field, $\mathbf{B}$ is the magnetic field, ϵ_0 is the electric constant, ρ_q is the density, μ_0 is the permeability of vacuum and $\mathbf{j}$ is the electric current. The ideal MHD equations consists of the continuity equation (Eq. 3.5), the momentum equation (Eq. 3.6), Ohm's law (Eq. 3.7) and the energy equation (Eq. 3.8). The conservation equations are:

$$\frac{\partial \rho}{\partial t} + \nabla \cdot (\rho \mathbf{v}) = 0 \tag{3.5}$$

$$\rho(\frac{\partial}{\partial t} + \mathbf{v} \cdot \nabla)\mathbf{v} + \nabla p - \mathbf{j} \times \mathbf{B} - \mathbf{f} - \mathbf{F}_{\text{visc}} = 0 \tag{3.6}$$

$$\mathbf{j} - \sigma(\mathbf{E} + \mathbf{v} \times \mathbf{B}) = 0 \tag{3.7}$$

$$\frac{\partial e}{\partial t} + (\mathbf{V} \cdot \nabla)e + \frac{p}{\rho}(\nabla \cdot \mathbf{V}) - \frac{1}{\rho}\nabla \cdot (\xi \rho \nabla e) - Q_{\text{visc}} - Q_{\text{Joule}} = 0, \tag{3.8}$$

where ρ is the mass density, $\mathbf{v}$ is the velocity field, p is the pressure, $\mathbf{F}_{\text{visc}}$ is the viscous force, $\mathbf{f}$ sums all other body forces, $\sigma = \frac{1}{\mu_0 \eta}$ is the conductivity, e is the inner energy, ξ is a thermal diffusivity, Q_{visc} and Q_{Joule} are viscous and Joule dissipations, and $\mathbf{E}$ and $\mathbf{B}$ are the electric and magnetic fields. A relation between the thermodynamic

quantities is needed to close the system of equations. The most used relation is that of the ideal gas, $p = nk_BT$, where n is the particle density, k_B is Boltzmann constant and T is the temperature.

Using Eq. (3.7) and Eq. (3.4) the term $\nabla \times \mathbf{E}$ takes the form

$$\nabla \times \mathbf{E} = \nabla \times (\eta \nabla \times \mathbf{B} - \mathbf{v} \times \mathbf{B}). \tag{3.9}$$

This can be substituted into Eq. (3.3) and one can derive the induction equation for the magnetic field:

$$\frac{\partial \mathbf{B}}{\partial t} = \nabla \times (\mathbf{v} \times \mathbf{B}) - \nabla \times (\eta \nabla \times \mathbf{B}). \tag{3.10}$$

If diffusive effects can be regarded to be small, i.e. $\sigma \to \infty$, $\eta \to 0$ in the system, we will get

$$\frac{\partial \mathbf{B}}{\partial t} = \nabla \times (\mathbf{v} \times \mathbf{B}), \tag{3.11}$$

which means that the plasma and magnetic field move together, in other words, the field is frozen into the fluid.

3.2.1 Mean-field approach

Stellar convective turbulence is extremely complex and beyond analytical techniques and accurate enough numerical modeling. Plasmas are also difficult to study in laboratories due to the extreme conditions required. Large-scale flows and magnetic fields are observed in the Sun and also in other stars, suggesting that a re-generative mechanism is needed to sustain the large-scale fields against turbulent diffusion. As both the length and timescales of the turbulent and large-scale phenomena can be expected to be vastly different, it has been proposed that a mean-field treatment of their evolution is possible without resolving, but parameterizing the effect of the small-scale turbulence. Such mean-field electrodynamics models were originally developed by Steenbeck *et al.* (1966), and used since the late 1960's. In these models, simple descriptions of turbulence and/or closure models are applied. The Reynolds numbers,

$$\mathrm{Re} = \frac{\mathrm{vL}}{\nu} \tag{3.12}$$

$$\mathrm{Rm} = \frac{\mathrm{vL}}{\eta}, \tag{3.13}$$

where v is a typical velocity of the flow, L is a length scale of the flow, ν is a kinematic and η the magnetic diffusivity, are dimensioless numbers that measure the relation between advection and diffusion. If Reynolds numbers are large, like in most space plasmas, advection dominates over diffusion. This leads to a highly turbulent state and effective mixing.

Turbulent effects, both diffusive and non-diffusive constributions, are often parameterized using simplifying assumptions, in order to find solutions to the MHD equations without solving the small-scale turbulence. Non-diffusive effects include for example the α-effect in the mean-field dynamo theory and the Λ-effect in the angular momentum transport theory. These effects make the mean-field approach a bit problematic. There are several higher-order terms in the equations of the dynamo processes, like in the equations (3.20) and (3.21), that need an appropriate closure. The most frequently used way is to remove all the fluctuations higher than the second-order. This method is called the first-order smoothing approximation (FOSA) or second-order correlation approximation (SOCA). The weakness of FOSA is that all the higher-order correlations are neglected from the fluctuations. The approximation fails if the fluctuations are large, like in many real turbulent systems.

The fundamental assumption made in the mean-field theory is that variables can be divided into their mean and fluctuating parts, i.e.

$$\mathbf{v} = \overline{\mathbf{v}} + \mathbf{v}', \tag{3.14}$$

where $\overline{\mathbf{v}}$ is an average of the quantity, in this case the velocity, and $\mathbf{v}'$ is the fluctuation for which $\overline{\mathbf{v}'} = 0$. The same can be done for the temperature and the magnetic fields, as well as current density and electric fields. Using this construction, the Ohm's law (3.7) takes the form

$$\bar{\mathbf{j}} + \mathbf{j}' = \sigma((\overline{\mathbf{E}} + \mathbf{E}')) + (\overline{\mathbf{v}} + \mathbf{v}') \times (\overline{\mathbf{B}} + \mathbf{B}'). \tag{3.15}$$

The Reynolds rules for averaging are:

$$\begin{aligned}
\overline{\overline{\mathbf{v}}} &= \overline{\mathbf{v}}, \\
\overline{\mathbf{v}'} &= 0, \\
\overline{\overline{\mathbf{v}}\mathbf{v}'} &= 0, \\
\overline{\overline{\mathbf{v_1}}\mathbf{v_2}} &= \overline{\mathbf{v_1}\mathbf{v_2}}, \\
\overline{\mathbf{v_1}\mathbf{v}_2} &= \overline{\mathbf{v_1}\mathbf{v}_2} + \overline{\mathbf{v}'_1\mathbf{v}'_2},
\end{aligned}$$

where $\mathbf{v_i} = \overline{\mathbf{v_i}} + \mathbf{v}'_\mathbf{i}$. When averaging over the Ohm's law, we get

$$\bar{\mathbf{j}} = \sigma(\overline{\mathbf{E}} + \overline{\mathbf{v}} \times \overline{\mathbf{B}} + \boldsymbol{\mathcal{E}}), \tag{3.16}$$

where a term

$$\boldsymbol{\mathcal{E}} = \overline{\mathbf{v}' \times \mathbf{B}'}, \tag{3.17}$$

called the mean electromotive force, appears due to the fluctuating fields. The fluctuating velocity field generates the fluctuating magnetic field, which influences the

plasma flow. The induction equation can be devided into its mean and fluctuating components in the same way:

$$\frac{\partial \overline{\mathbf{B}}}{\partial t} + \frac{\partial \mathbf{B}'}{\partial t} = \nabla \times (\overline{\mathbf{v}} \times \overline{\mathbf{B}} + \mathbf{v}' \times \overline{\mathbf{B}} + \overline{\mathbf{v}} \times \mathbf{B}' + \mathbf{v}' \times \mathbf{B}') \\ -\nabla \times \eta \nabla \times \overline{\mathbf{B}} - \nabla \times \eta \nabla \times \mathbf{B}'. \tag{3.18}$$

After averaging, the equation for the mean field reads:

$$\frac{\partial \overline{\mathbf{B}}}{\partial t} = \nabla \times (\overline{\mathbf{v}} \times \overline{\mathbf{B}} + \boldsymbol{\mathcal{E}} - \eta \nabla \times \overline{\mathbf{B}}) \tag{3.19}$$

The equation for the fluctuating component can be obtained by substracting (3.19) from (3.18) and reads:

$$\frac{\partial \mathbf{B}'}{\partial t} = \nabla \times (\mathbf{v}' \times \overline{\mathbf{B}} + \overline{\mathbf{v}} \times \mathbf{B}' + \mathbf{v}' \times \mathbf{B}' - \boldsymbol{\mathcal{E}} - \eta \nabla \times \mathbf{B}'). \tag{3.20}$$

If $\mathbf{B}'$ is small enough, which occurs if the Reynolds number or the Strouhal number, which can be regarded to be a non-dimensional measure of the correlation time of the turbulence, is small, only the first right-hand side term of the Eq. (3.20) is left (see Eq. 3.21). This is the FOSA/SOCA approach to the induction equation, according to which $\mathbf{B}'$ differs from the mean field at the time τ

$$\mathbf{B}' \approx \tau \nabla \times \mathbf{v}' \times \overline{\mathbf{B}} \approx \tau (\overline{\mathbf{B}} \cdot \nabla) \mathbf{v}' - \tau (\mathbf{v}' \cdot \nabla) \overline{\mathbf{B}}. \tag{3.21}$$

Because of the linear relation between the fields $\overline{\mathbf{B}}$, $\mathbf{B}'$ and $\boldsymbol{\mathcal{E}}$, the electromotive force can be developed as a rapidly convergent series of the form

$$(\mathbf{v}' \times \mathbf{B}')_i = \epsilon_{ijk} v_j' B_k' = \epsilon_{ijk} v_j' \overline{B}_l \frac{\partial v_k'}{\partial x_l} \tau - \epsilon_{ijk} v_j' v_l' \frac{\partial \overline{B}_k}{\partial x_l} \tau + ..., \tag{3.22}$$

If this is averaged and the places of summing indexes j and l are changed and FOSA is used, the i:th component of mean electromotive force gets the form

$$\mathcal{E}_i = \alpha_{ij} \overline{B}_j + \beta_{ijk} \frac{\partial \overline{B}_k}{\partial x_j}, \tag{3.23}$$

where

$$\alpha_{ij} = \epsilon_{ijk} \overline{v_l' \frac{\partial v_k'}{\partial x_j}} \tau, \qquad \beta_{ijk} = -\epsilon_{ilk} \overline{v_l' v_j'} \tau \tag{3.24}$$

are pseudotensors, which may be expected to depend on $\overline{\mathbf{v}}$ and $\mathbf{v}'$. When the flow is helical, and if the turbulence is considered as isotropic and homogenous, the tensors (3.24) take the simpler form

$$\alpha_{ij} = \alpha \delta_{ij}, \qquad \beta_{ijk} = -\eta_t \epsilon_{ijk}\,, \tag{3.25}$$

where δ_{ij} is the Kronecker-tensor and η_t is the enhanced turbulent diffusivity. The mean electromotive force can thus be written into the form

$$\boldsymbol{\mathcal{E}} = \alpha\overline{\mathbf{B}} - \eta_t \nabla \times \overline{\mathbf{B}}, \tag{3.26}$$

where α is a pseudoscalar and η_t is a scalar, because η is small in comparison, so $\eta + \eta_t \sim \eta_t$. The induction equation for the mean-field magnetic field can be written

$$\frac{\partial \overline{\mathbf{B}}}{\partial t} = \nabla \times (\overline{\mathbf{v}} \times \overline{\mathbf{B}} + \alpha\overline{\mathbf{B}}) - \nabla \times (\eta_t \nabla \times \overline{\mathbf{B}}). \tag{3.27}$$

Eq. (3.27) is also called the dynamo equation. The coefficient α describes the generation of the poloidal component from the toroidal component by helical turbulence. This term would go to zero if the turbulence had no net average helicity (which would happen in a non-rotating frame). The coefficient η_t is a diffusion coefficient induced by turbulence. If the magnetic Reynolds number is large, i.e. in the limit Rm >> 1, the fluctuating field $\mathbf{B}'$ can be determined from the equation (e.g. Krause and Rädler, 1980)

$$\mathbf{B}' = \int_{-\infty}^{t} \nabla \times (\mathbf{v}' \times \overline{\mathbf{B}} dt'), \tag{3.28}$$

resulting in

$$\alpha = -\frac{1}{3}\int_0^\infty \overline{\mathbf{v}' \cdot (\nabla \times (\mathbf{v}'(t-t')))} dt' = -\frac{1}{3}\overline{\mathbf{v}' \cdot (\nabla \times \mathbf{v}')\tau_{\rm corr}}, \tag{3.29}$$

and

$$\eta_t = \frac{1}{3}\int_0^\infty \overline{\mathbf{v}' \cdot \mathbf{v}'(t-t')} dt' = \frac{1}{3}\overline{\mathbf{v}'^2}\tau_{\rm corr}. \tag{3.30}$$

Obviously, we have so far treated only the two first terms in the series expansion of the electromotive force. This is the most simple and most commonly used closure of the mean-field equations.

3.2.2 Nonlinear saturation

The magnetic fields that are generated in the dynamo processes will eventually produce a Lorentz force that will act against the driving fluid motions. This effect should be added to all dynamo models, but this is not trivial, because turbulence can affect both the large-scale flow components as well as the small-scale turbulent flow providing turbulent stresses powering the large-scale flows. Most dynamo models are kinematic, where the magnetic field grows unlimited, so those models do not give the strength of the magnetic field. The standard way of thinking is that the field growth via the α-effect becomes non-linearly affected by the growing magnetic field, so that the α-effect is quenched and the field growth saturates when the magnetic field becomes dynamically important, i.e. the magnetic energy grows to be equally

large as the kinetic energy of turbulence. The classic algebraic α-quenching can thus be formulated as:

$$\alpha = \frac{\alpha_0}{1 + (\frac{B}{B_{\rm eq}})^2}, \tag{3.31}$$

where α_0 is the unquenched value and $B_{\rm eq}$ is the equipartition value of magnetic field with respect to the kinetic energy of turbulent motions. According to e.g. Cattaneo and Vainshtein (1991) the magnetohydrodynamic turbulent dynamo will stop operating as soon as the relation $\mathbf{B'}^2 = {\rm Rm}\overline{\mathbf{B}^2}$ is satisfied, a process that can happen in much shorter time than the turbulent eddy turnover time. This will lead to the catastropich quenching, i.e. a strong decrease of α already for weak mean fields in the limit of large Rm in a closed system. This behavior would imply that the mean-field dynamos driven by the α-effect could not generate the observed large-scale magnetic fields in cosmical objects, casting doubt on the whole dynamo scenario.

The magnetic helicity in mathematical formulation is defined as a surface integral over a closed or periodic volume V

$$H_m = \int_V \mathbf{A} \cdot \mathbf{B} dV, \tag{3.32}$$

where $\mathbf{A}$ is the vector potential, related to the magnetic field via $\mathbf{B} = \nabla \times \mathbf{A}$. Magnetic helicity describes how globally sheared or twisted the magnetic field is in a certain volume. This quantity is believed to play a key role in solar and stellar activity due to its conservation property (e.g. Brandenburg and Subramanian, 2005),

$$\frac{dH_m}{dt} = \int_V (\mathbf{A} \cdot \frac{\partial \mathbf{B}}{\partial t} + \mathbf{B} \cdot \frac{\partial \mathbf{A}}{\partial t}) dV = -2 \int_V \eta \mathbf{B} \cdot \nabla \times \mathbf{B} dV + {\rm S},$$

where S represents the surface terms. From here it can be seen that in the non-resistive case, i.e. $\eta = 0$, magnetic helicity is conserved as $\frac{d{\rm Hm}}{dt} = 0$. The basic physical idea is that due to the magnetic helicity conservation the production of helicity in the mean field implies a corresponding production of helicity of opposite sign at the scales of the fluctuating components of the flow and the field. This production ends up acting in a way that it reduces the α-effect and it can be shown to become time-dependent (Brandenburg and Subramanian, 2005):

$$\frac{d\alpha}{dt} = -2\eta_t k_f^2 (\frac{\alpha \overline{\mathbf{B}}^2 - \eta_t \bar{\mathbf{j}} \cdot \overline{\mathbf{B}}}{B_{\rm eq}^2} + \frac{\alpha - \alpha_K}{\rm Rm}). \tag{3.33}$$

To keep the dynamo working at high Rm there must be a way to get rid of the small-scale magnetic helicity otherwise suffocating the dynamo process. This can be achieved if helicity fluxes occur, e.g. when the dynamical α-effect gets the form

$$\frac{d\alpha}{dt} = -2\eta_t k_f^2 (\frac{\alpha \overline{\mathbf{B}} - \eta_t \bar{\mathbf{j}} \cdot \overline{\mathbf{B}} + \frac{1}{2} k_f^{-2} \nabla \cdot \mathbf{F_C}}{B_{\rm eq}^2} + \frac{\alpha - \alpha_K}{\rm Rm}), \tag{3.34}$$

where $\mathbf{F_C}$ represents a helicity flux, which could be provided for example by coronal mass ejections (e.g. Brandenburg *et al.*, 2009, and references therein).

Magnetic helicity studies have become an important tool to describe the complexity of the Sun's magnetic field. H_m is practically a non-observable quantity and current helicity is used as a proxy. Satellite measurements of the solar wind also provide some information on Sun-induced H_m in the interplanetary space (e.g. Brandenburg *et al.*, 2011b). Vector magnetograms of active regions can also be used to measure current helicity. Chae (2000) estimated the magnetic helicity flux by counting the crossings of pairs of flux-tubes close to each other. With the assumption that two flux-tubes are nearly aligned, Chae (2000) suggested that the magnetic helicity is negative in the Northern Hemisphere and positive in the Southern Hemisphere. DeVore (2000) found the same sign distribution and concluded that magnetic helicity is generated due to differential rotation. Démoulin *et al.* (2002) discovered that oppositely signed twists and writhes can produce a small total magnetic helicity which leads to bi-helical fields.

Shear flows have been argued to be responsible of alleviating catastrophic quenching (Vishniac and Cho, 2001), and making it possible to get significant saturation levels of the dynamo (Käpylä *et al.*, 2008). Recent direct numerical simulations by Hubbard and Brandenburg (2011, 2012), however, have failed to show the importance of the Vishniac-Cho flux. The more recent simulations by Del Sordo *et al.* (2013) have, however, demonstrated the importance of advective helicity fluxes, that can originate from winds/outflows. These simulations were driven by subsonic flows, but in real astrophysical objects the outflows can be supersonic and thus this effect can play even more important role reducing the catastrophic quenching.

3.3 Solar and stellar dynamos

The dynamo mechanism converts kinetic energy into magnetic energy and the energy for the solar dynamo comes from nuclear reactions in the center of the Sun. The thermal energy is converted into kinetic energy through the convective instability. In 1919, Larmor suggested that the inductive action of fluid motions could be an explanation for the origin of the solar magnetic field, thus opening the first era for modeling of the solar magnetic activity (Charbonneau, 2010). Two decades later Cowling defeated Larmor's idea by showing that even the most general, purely axisymmetric, flows could not sustain an axisymmetric magnetic field against Ohmic dissipation (Cowling, 1934). This result is known as Cowling's antidynamo theorem. A solution to this antidynamo theory was only discovered in the mid-1950's, when Parker showed that the Coriolis force could pass on a systematic cyclonic twist to rising turbulent fluid elements in the solar convection, and when doing so, break-

ing the total axisymmetry and thus avoiding the Cowling's theorem. Parker's model opened a new era for understanding the basis of the solar activity cycle, and later on its mathematical foundation utilizing mean-field electrodynamics was provided by Steenbeck *et al.* (1966).

All solar dynamo models have a common basis, most importantly a differential rotation profile, and a magnetic diffusivity profile, that might possibly be depth-dependent. The most often used mean-field dynamo models work under the so-called kinematic approach, where the velocity field is assumed given, and utilize the algebraic α-quenching formula (Eq. 3.31). The main differences arise in how the turbulent quantities are described (Charbonneau, 2010). It is possible to separate solar dynamos to work under two different paradigms, namely the distributed dynamo, emphasizing the role of turbulent convection throughout the convection zone, and flux-transport dynamos that regard convection largely unimportant and emphasize the role of the shear layers and the meridional circulation connecting the tachocline shear and the surface magnetic field amplification layer (Charbonneau, 2010). These models are discussed in the next two subsections.

When the Sun was young it rotated more rapidly than it does today. Observations of young, rapidly rotating stars indicate that many have substantial magnetic activity, many of the stars showing cyclic changes in the activity level and strong non-axisymmetric magnetic field component. The fact that the late-type stars show magnetic cycles is the strongest proof for a dynamo operating in the convection zones; stable magnetic field configurations such as those seen in early-type hot stars indicate fossil fields slowly diffusing in the outer radiative zone. In mean-field theory, both generation terms are sensitive to rotation, the α-effect because it is proportional to the kinetic helicity of the convective flows, and the Ω-effect because streching and winding out the field lines are caused by differential rotation. Most solar dynamo models have been carried out in 2-D using the simplifying assumptions of the mean-field theory (e.g. Küker and Stix, 2001, and references therein). For rapidly rotating stars full 3-D simulations of global-scale stellar convection are needed to understand the complex coupling between rotation, convection and magnetism and arising non-axisymmetric magnetic field configurations. Many cool stars have enhanced activity levels, suggesting the presence of stronger surface magnetic fields produced by more efficient dynamos. Dynamos in cool stars usually give rise to topologically complex magnetic fields.

3.3.1 The distributed solar dynamo

Parker suggested in his seminal paper in 1955 that solar magnetism and magnetic activity was created by a dynamo process. Parker (1955) introduced an axisymmetric

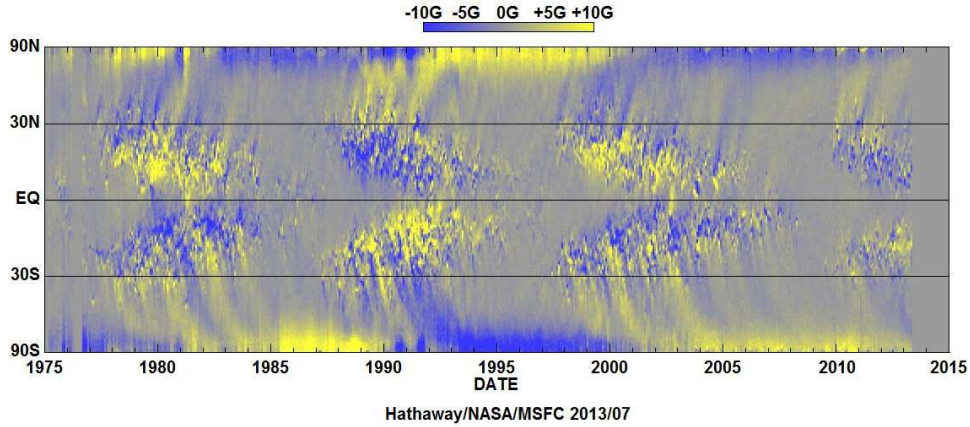

Figure 3.1: Synoptic magnetogram of the radial component of the solar surface magnetic field. The low latitude component is associated with sunspots (Image Credit: D. Hathaway, NASA/MSFC).

model working at the high-Rm limit, where the magnetic field is nearly frozen in the plasma (molecular diffusivity is negligible) and turbulent convection is significant for the magnetic field in the whole convection zone.

Parker's dynamo model consists of a dynamo cycle, in which a poloidal and toroidal magnetic fields sustain each other. The toroidal field arises due to the action of differential rotation on the poloidal field (Ω-effect), and the dynamo cycle is completed when poloidal field is generated back from the toroidal field by helical turbulence (α-effect). The latter effect arises when the Sun's rotation causes twisting of the magnetic field lines due to the Coriolis force, which also makes sunspot groups to obey Joy's law, and results in the appearance of small-scale poloidal field loops. The small poloidal field entities then reconnect to larger and larger structures due to the action of the enchanced turbulent diffusion, $\eta_{\rm t}$, finally generating large-scale poloidal field with a reversed sign.

The dynamo equation (3.27) was originally written in Cartesian coordinates, the coordinate ϕ being the azimuthal angle (longitude) in the xy-plane from the x-axis with $0 \leq \phi < 2\pi$, ϑ the polar angle, with $\vartheta = 90^\circ - \theta$ where θ is the latitude from the positive z-axis with $0 \leq \vartheta \leq \pi$, and r being the distance (radius) from a point to the origin. The coefficients $\alpha(r, \theta)$ and $\Omega(r, \theta)$ and their axisymmetric spatial profile are assumed to be known. Symmetry properties versus the equator require that α is antisymmetric and Ω is symmetric with respect to the equator. The α-effect is capable of generating a mean magnetic field, but in the case of most stars the more

interesting solutions are in combination with the differential rotation.

$$\begin{aligned} \alpha(r, \pi - \theta) &= -\alpha(r, \theta)\,, \\ \Omega(r, \pi - \theta) &= \Omega(r, \theta). \end{aligned}$$

The mean rotational velocity can be written with the help of the mean rotational velocity of the plasma,

$$\overline{\mathbf{V}} = (0, 0, \Omega r \sin\theta).$$

The mean magnetic field is split into poloidal and toriodal components $\overline{\mathbf{B}} = \mathbf{B}_\mathrm{p} + \mathbf{B}_\mathrm{t}$. The poloidal component can be expressed as a vector potential, which leads to

$$\begin{aligned} \mathbf{B}_\mathrm{p} &= \nabla \times (0, 0, A(r, \theta, t))\,, \\ \mathbf{B}_\mathrm{t} &= (0, 0, B(r, \theta, t)). \end{aligned}$$

The same decomposition can be applied to the mean-field induction equation, which leads to, in the simplest case when η_t is a constant,

$$\frac{\partial A}{\partial t} = \alpha B + \eta_t \nabla_1^2 A \tag{3.35}$$

$$\begin{aligned} \frac{\partial B}{\partial t} &= \frac{\partial \Omega}{\partial r}\frac{\partial}{\partial \theta}(A \sin\theta) - \frac{1}{r}\frac{\partial \Omega}{\partial \theta}\frac{\partial}{\partial r}(rA\sin\theta) \\ &- \frac{1}{r}\frac{\partial}{\partial r}\left[\alpha \frac{\partial}{\partial r}(rA)\right] - \frac{1}{r^2}\frac{\partial}{\partial \theta}\left[\frac{\alpha}{\sin\theta}\frac{\partial}{\partial \theta}(A\sin\theta)\right] + \eta_t \nabla_1^2 B\,, \end{aligned} \tag{3.36}$$

where Eq. (3.35) is a poloidal component and Eq. (3.36) is a toroidal component and $\nabla_1^2 = \nabla^2 - (r\sin\theta)^{-2}$. Equations (3.35) and (3.36) show how crucial role the α-effect has in the kinematic dynamo theory. With $\alpha = 0$, the poloidal field would decay exponentially, because the left-over is a diffusion equation. And with A gone, B would decay as well, for the same reason. The source term for the poloidal field involves α and the source term for the toroidal field involves both α and Ω. If Ω-effect is much stronger than the α-effect, the α-term in Eq. (3.36) can be neglected and the dynamo is said to be of $\alpha\Omega$ type. In solar models the α-effect is often neglected in this equation, if the condition $|\alpha| << r_\mathrm{Sun}^2 |\nabla\Omega|$ is met. The magnitude of α is not known exactly, but most likely this condition meets the requirements.

If a late-type star does not have much differential rotation, the dynamo will be an α^2-dynamo in which case both the toroidal and poloidal component are generated by the α-effect (in Eq.s (3.35) and (3.36) the Ω-term is small or vanishes). Dynamos of some rapidly rotating stars are believed to be of this kind. The magnetic fields produced by the very simplest α^2-dynamos were shown to be steady in time (e.g. Krause and Rädler, 1980), although it was already early realised that any sign-changes in the α-effect, for example, could lead to oscillatory solutions (e.g. Baryshnikova and

Shukurov, 1987; Rüdiger *et al.*, 2003; Mitra *et al.*, 2010). For decades, however, only the results from the simplest models have been regarded important, which has lead to the misconception that all α^2-dynamos would be steady in time. Recently, many new studies showing that oscillatory solution as actually possible have been published, see e.g. Käpylä *et al.* (2013, and references therein). The dynamo is an $\alpha^2\Omega$-dynamo if both the α-effect and differential rotation contribute to the toroidal field production.

After developing the basic kinematic dynamo theory, Parker (1955) showed that the dynamo equation (3.27) allows a periodic wave solution when there is differential rotation. Dynamo waves travel in a direction s given by:

$$s = \alpha \nabla \Omega \times \hat{e}_\phi, \tag{3.37}$$

which is nowadays called as the Parker-Yoshimura sign rule. The dynamo equation gives solutions for the poloidal (A) and for the toroidal (B) terms. These fields can move either polewards or equatorwards (Yoshimura, 1975). If the α-effect and the gradient of Ω have the same sign, this means polewards migration in the Northern Hemisphere. If they have different signs, migration is equatorward as observed (Fig. 3.1). Sunspots are considered to be produced in the regions where the wave has its peak. The equatorward propagation of the peak gave an explanation why sunspots appear at progressively lower latitudes as the cycle advances. This was later proved to hold in spherical geometry, as well as in non-linear models (Yoshimura, 1975).

Simple kinematic mean-field models show that when rotation rate is increasing, and the relative amplitude of the α-effect vs. the Ω-effect is increasing, the preferred solutions change from the axisymmetric ones to the non-axisymmetric ones (Krause and Rädler, 1980). The non-axisymmetric modes generated by α^2- or $\alpha\Omega$-dynamos are characterized by East- or Westward migration with respect to basic rotation rate, i.e. azimuthal dynamo waves (Krause and Rädler, 1980). The dynamo waves can be slow or fast depending on the profile and properties of the turbulent transport coefficients. It has also been discussed, from a more phenomenological point-of-view, that magnetic flux-tubes arising from the bottom of the convection zone become the more strongly deflected towards high latitudes, the stronger is the Coriolis force (e.g. Schüssler and Solanki, 1992). These theoretical predictions are in agreement with the observational results (e.g. Strassmeier, 1990; Donati *et al.*, 1992; Hatzes *et al.*, 1996) bar that the flip-flop type phase jumps are not explainable by either of the extreme cases of $\alpha\Omega$- or α^2-dynamos. It has been suggested by e.g. Elstner and Korhonen (2005) that such behavior would be a result of the competition of axisymmetic and nonaxisymmetric dynamo modes in a model reminescent of a $\alpha^2\Omega$-model.

If the α-effect is created by the twisting of magnetic fields due to the Coriolis-force, it will be positive in the Northern Hemisphere and negative in the Southern Hemisphere. This would imply a need for a negative radial gradient of Ω, but as seen

in Fig. (2.4), the gradient is positive in the majority of the convection zone, except for the shear layers. The first numerical simulations of turbulent thermally-driven convection in a thick rotating spherical shell showed magnetic field migration patterns that did not look like the ones that had been observed (e.g. Gilman, 1983). The first determinations of the Sun's internal differential rotation came when helioseismology opened the new era for solar studies Howe (e.g. 2009, and references therein). As illustrated in Fig. (2.4), the gradient of Ω is positive in the bulk of the convection zone, with regions of strong shear. These findings would predict wrong migration properties when utilizing the Parker-Yoshimura rule, and this is actually the case with Parker-type simple dynamo models. Käpylä *et al.* (2005) calculated the α-tensor from local turbulent convection models, as a function of latitude and radius, and showed that the profiles are all but simple. The α-profile changed sign as a function of latitude and was a lot steeper than the cos-profile. Käpylä *et al.* (2006, 2009) also showed that a solar-like dynamo solution was possible to produce by using the obtained α-profiles with meridional circulation and the rotation profile obtained from helioseismology.

3.3.2 Flux-transport dynamos

Flux transport dynamos got popular during the deep descent of classical, distributed dynamo theory due to the problems related to the incorrect migration and catastrophic quenching in the nonlinear regime. In this type of models, both the observed equatorward migration of sunspot source regions and poleward migration of surface fields are driven by the meridional flow. The cycle period can be set by the meridional flow speed. This kind of dynamos reproduce quite well and robustly many observed solar cycle features.

Babcock (1961) introduced a five-stage magnetic cycle model that reproduces the Sun's magnetic cycle. The initial stage of the Babcock-model describes the Sun's magnetic field in an axisymmetric dipolar configuration where the field lines are in the meridional plane. The magnetic field lines emerge from the north pole and reconnect at the south pole. Because of this axisymmetric dipolar field geometry, the solar surface is affected by the magnetic field at latitudes of $\pm 55^\circ$ or greater. In a three year period the field lines are drawn out and twisted by differential rotation until they are almost east-west oriented along the solar equator (Charbonneau, 2010). Together with rotation the convection shapes the orientation of field lines to an almost toroidal configuration, to the critical field intensity. The location of the critical field intensity in the magnetic cycle processes is calculated as:

$$\sin\theta = \pm\frac{1.5}{n+3}, \tag{3.38}$$

where θ is the latitude and n is the number of years since the beginning of the 11 years sunspot cycle. This equation is also known as Spörer's law for the variation of

sunspot latitude.

Flux-tubes continue to rise and erupt at the surface until the magnetic field pressure reaches the level of the gas pressure. This allows the emergence of the flux-tubes at the surface forming larger sunspot pairs, bipolar magnetic regions, and when the strength of the flux-tubes is high enough to suppress the convection, sunspots are forming. The first appearance of sunspots of different polarities defines the starting point of the new 11 years sunspot cycle and the cycles may overlap. When the sunspot cycle approaches its maximum, the gas pressure defeats the magnetic pressure. Surface differential rotation together with the Coriolis force causes the sunspot pairs with bipolar magnetic regions to migrate in separate directions. The leading spot is moving toward the equator and the following spot is migrating poleward. As these pairs move away from each other, their magnetic field lines stretch and break and thus reconnect with the existing main dipolar field that extends from the poles. This allows plasma that was frozen into the magnetic field to be ejected into the solar corona. The broken field lines also reconnect at the surface but with reversed polarity. Flux-tubes under the solar surface in the influence of the differential rotation, return the magnetic field to a meridional orientation, and due to their reversed polarity, the main dipolar field also changes polarity.

In 1969 Leighton (1969) explained the poleward migration of the following sunspots in bipolar magnetic regions in the Babcock-model being a random walk process and the asymmetry of the eruption of the flux-tubes due to the Sun's rotation. This kinematic model is thus called a Babcock-Leighton dynamo model. Because of the strong amplification of the surface poloidal field in the poleward converging meridional flow, the Babcock-Leighton models quite often produce a significant and often dominant polar branch in the toroidal field butterfly diagram.

Stability studies of toroidal flux-ropes stored in the overshoot layer have been done using a thin-flux-tube approximation (Spruit, 1981). If the diameter of a magnetic flux-tube is much smaller than any other length scale, the MHD equations connected to its evolution can be simplified in terms of the thin-flux-tube approximation. It is possible to create stability diagrams taking the form of growth rate contours in a parameter space comprised of flux-tube strength, latitudinal location, and depth in the overshoot layer. The observed properties of the magnetic field in the solar photosphere and theoretical studies of magneto-convection in conducting fluids suggest that the magnetic field in stellar convection zones is quite inhomogeneous (e.g. Charbonneau, 2010, and references therein). Magnetic flux is concentrated into magnetic flux-tubes embedded in significantly less magnetized plasma, although this kind of flux-tubes have not been seen yet in direct numerical simulations (e.g. Charbonneau, 2010, and references therein).

The storage of magnetic flux for periods that are comparable to the amplification time of the dynamo requires the compensation of the magnetic buoyancy. Flux-tubes stored in a mechanical force equilibrium in the overshoot layer become unstable once a critical field strength is exceeded. Flux-loops then rise through the convection zone and erupt as bipolar magnetic regions at the surface. Parameter values that are relevant for the solar case, need a critical field strength of the order of 10^5 G. A field of similar strength is also required to prevent the rising unstable flux-loops from being deflected poleward by the action of the Coriolis force and also from bursting in the middle of the convection zone (Schüssler and Ferriz-Mas, 2003). The instability of magnetic flux-tubes stored in the overshoot region suggests a dynamo mechanism that is based on growing helical waves propagating along the tubes. Because this process only operates for field strengths reaching a critical value, a dynamo can fall into a grand minimum once the field strength is globally driven below this value, for instance by magnetic flux pumped at random from the convection zone into the dynamo region in the overshoot layer. The same process may act as a starting point of the dynamo operation (Schüssler and Ferriz-Mas, 2003).

The bipolar magnetic regions often emerge with a systematic tilt in the east-west direction, so that the leading sunspot with respect to the solar rotation is located at a lower latitude than the trailing sunspot. This pattern, which is referred to as Joy's law, is caused by the influence of the Coriolis force on the secondary azimuthal flow developing within the rising magnetic toroidal flux-rope which produces a bipolar magnetic region. This tilt is the key of the Babcock-Leighton mechanism for polar field reversal. Mathematically the Babcock-Leighton mechanism can be formulated as the surface distribution of the radial magnetic field associated with a bipolar magnetic region ($B_r^\theta = (\theta, \phi)$).

The leading spot of the bipolar magnetic region is located closer to the equator. The spot experiences a bigger diffusive cancellation across the equatorial plane with the opposite polarity leading spots of the other hemisphere, than the trailing spots. The plasma near the Sun's surface continuously flows from the equator to the pole, with a maximum flow speed of about 20 m/s in the mid-latitudes. This is known as the meridional circulation. In the decay stage, the magnetic flux of the trailing spot is transported to the polar region by supergranular diffusion and the surface meridional flow. The matter brought from the equatorial region to the polar region by the meridional circulation has to be returned back, to avoid a gradual pile-up of matter near the poles. It is usually believed that the meridional circulation is driven by the turbulent stresses in the convection zone.

The Babcock-Leighton process can be described with the help of the coefficient α concentrated near the solar surface. In analogy with mean-field theory, the α-effect

is considered to be proportional to kinetic helicity but of opposite sign, and ends up predominantly positive at mid-latitudes in the Northern solar Hemisphere. The dynamos using the Babcock-Leighton mechanism are not self-excited, because the required tilt of the emerging bipolar magnetic region only materializes in a range of toroidal field strength from a few 10^4 G to about 2×10^5 G (Charbonneau, 2010). The α-effect is also concentrated on the surface and the turbulent diffusion must be smaller of the order of a unity, so that the models work.

Dikpati and Gilman (2001) use a solar-like differential rotation, and depth-dependent magnetic diffusivity in their dynamo model. These models manage to reproduce a number of observed solar cycle features. The model can be adjusted to produce equatorward propagating dominant activity belts, solar-like cycle periods, and correct phasing between the surface polar field and the tachocline toroidal field. These features can be traced to the advective action of the meridional flow. They also give the correct parity of the solution, and are self-excited. The weakness in this model is the reliance on a linear stability analysis that ignores the destabilizing effect of magnetic fields, that the meridional circulation is only one-celled, and the turbulent diffusion is kept low in comparison to what has been estimated from direct numerical simulations (e.g. Karak *et al.*, 2014, and references therein).

3.4 Stellar rotation and its non-uniformities

The Sun is known to rotate differentially since Carrington (1863): the angular velocity increases from the poles towards the equator. Now, about 150 years after the discovery, the origin of the differential rotation is quite well understood theoretically. Numerical models based on the theory reproduce solar rotation and predictions for the differential rotation of other stars are to some extent confirmed by observations.

The change from the rigid rotation of the core to the latitudinally and radially changing rotation in the convection zone can be explained by the different angular momentum transport mechanisms. The Sun has a weak gradient in the convection zone, and strong shear layers in the tachocline and near the surface. The diffusion time-scale in the core of the Sun is long, suggesting that the solid rotation could have been created by a weak, primordial magnetic field (e.g. Kitchatinov and Rüdiger, 2006). The diffusion time-scale in the convection zone is shorter (order of 10^2), which suggests that there is a process that constantly re-generates differential rotation. In the mean-field theory of stellar rotation the angular momentum transport in the convection zone is formed due to the off-diagonal components of the Reynolds stress tensor arising from turbulent convection. The Reynolds stresses influence the meridional flow directly as well as indirectly with the differential rotation itself. The meridional circulations has been proposed to be especially important for the dynamo

process; the prevailing flux-transport dynamo paradigm even bases its operation on one-single meridional circulation cell. In the Northern Hemisphere, the flow direction is observed to be directed from from the equator to the poles at the top of the convection zone, and the flow direction is assumed to be reversed in the deeper layers, which argument arises from the requirement for conservation of mass and from the fact that no excess of matter is observed to accumulate to polar regions (e.g. Pipin and Kosovichev, 2013, and references therein). Anisotropic turbulent heat transport can create a pole-equator temperature difference, which can also drive meridional circulation anisotropized by rotation and stratification, and in the non-linear regime by magnetic fields.

The generation of stellar differential rotation can be studied either by mean-field modeling by averaging the Navier-Stokes equation (analogously to mean-field dynamo theory, see e.g. Rüdiger (1989), or by direct numerical simulation either on local (Käpylä *et al.*, 2004) or global scale (e.g. Matt *et al.*, 2011; Käpylä *et al.*, 2011a,b; Käpylä, 2011). Antisolar profiles have been found for stars slightly more massive than the Sun (e.g. Matt *et al.*, 2011) and for sufficiently intensive meridional circulation (e.g. Kitchatinov and Rüdiger, 2004). For the solar-type stars, if $\Omega < \Omega_{\rm Sun}$, and the shear parameter is negative, the differential rotational profiles are anti-solar type, i.e. the polar regions rotate faster than the equator, whereas e.g. if $\Omega > \Omega_{\rm Sun}$, the profile is solar-like (Käpylä *et al.*, 2011a,b). Also the observations give support to this prediction (e.g. Collier Cameron *et al.*, 2002; Strassmeier *et al.*, 2003; Weber *et al.*, 2005). If Ω is high, meaning that the Coriolis force is also high, the differential rotation first becomes smaller, and then stays constant (e.g. Käpylä *et al.*, 2011b).

The mean-field models (e.g. Kitchatinov and Rüdiger, 1999) predict that the magnitude of the relative differential rotation, indeed, is weakly decaying as a function of increasing rotation rate $k \sim \Omega$. Stellar differential rotation is a large-scale phenomenon, so it is possible to study internal rotation of stars with the help of the mean-field theory by averaging the Navier Stokes equations (e.g. Rüdiger, 1989, and references therein). Simulations of global circulation in outer stellar convection zones for spectral classes G2 and K5, rotating at the same rate, show that differential rotation for G2 is higher compared to K5 (Kitchatinov and Rüdiger, 1999). The magnetic field is stored in the deep interior, if a strong magnetic diffusivity gradient exists between the core and the envelope. Rapid rotation can explain the strong total surface differential rotation of young solar-type stars, as it creates meridional flow on the stellar surface, which accelerates the equatorial rotation (Rüdiger and Küker, 2002). Shear flows also have a big role in many hydromagnetic dynamo models, especially in the solar ones.

3.5 Current trends

Modeling the evolution of the Sun's surface magnetic flux has confirmed that the Babcock-Leighton mechanism is operating in the Sun. The past 30 years the solar dynamo has mostly been placed at the bottom of the convection zone or in the overshoot layer. This region is called the tachocline. Magnetic fields that are freed by the decay of tilted bipolar active regions gather together in the polar regions, where they drive the polarity reversal of the poloidal component (e.g. Baumann *et al.*, 2004). The problem is whether this is an active component of the dynamo cycle or a side effect of the active region decay. This leads to a question if the sunspot butterfly diagram should be interpreted in terms of the Parker-Yoshimura sign rule or advection by meridional circulation. The main question regarding meridional circulation in the Sun is not whether it is there or not, but rather what role it plays in the solar cycle. The answer is hidden in the value of the turbulent diffusivity, which is obviously difficult to estimate with confidence.

There are still many theoretical facts contradicting the flux-transport models. The arguments favouring flux-transport dynamos operating in the tachocline are flux storage and weak turbulent distortions. These models also manage to reproduce the correct butterfly diagram with meridional circulation, and the sizes of active regions are naturally explained (Brandenburg, 2005). But problems still remain, like how to produce the 100 kG fields needed for the standard scenario of an overshoot dynamo. Other arguments against the flux-transport models are flux-tube integrity during ascent and that the models produce too many flux-belts in latitude. Also the maximum radial shear is at the poles, and very little radial shear exists where the sunspots show up. These models prefer quadrupolar parity, and produce a wrong phase relation and require a coherent convey or belt-like meridional circulation pattern. The general problem in the Babcock-Leighton models is the specification of an appropriate poloidal source term, to be incorporated into the mean-field axisymmetric dynamo equations. In all cases so far published the poloidal source term is concentrated in the outer convective envelope, leading to a positive α-effect. The Babcock-Leighton dynamo models produce strong polar surface magnetic fields, that can be fixed by increasing the magnetic diffusivity close the surface layers. This leads to a much weaker poloidal field, which is transported down to the tachocline.

According to the flux-transport paradigm the poleward plasma flow transports the surface magnetic flux from low latitudes to the polar region reversing the global magnetic field. More accurate measurements of the flow speeds have been done by Zhao *et al.* (2013) who claim a change of sign of the meridional flow at 0.82 $R_{\rm Sun}$, shallower than previously thought, indicating that the pattern may consist of more than a one cell. In simulations the models with the solar-like differential rotation tend

to produce multiple cells of meridional circulation, when the models with anti-solar differential rotation produce only one or two meridional cells (e.g. Guerrero *et al.*, 2013), which violates the standard flux-transport model. Arlt *et al.* (2007) studied the stability of the tachocline, reporting mildly turbulent tachocline conditions, where differential rotation alone is either stable or very slightly supercritical. There is only a limited way to store toroidal magnetic fields in the tachocline and the models of thin flux-tube rise require strong fields of 100 kG in order to reproduce the low latitude sunspots and the tilt angle of bipolar groups.

The whole sunspot phenomenon may be rather more shallow than suggested by the standard picture. An overall decrease of the electromotive force also has to be taken into account while using flux-transport models. An overall decrease of the electromotive force could occur because of magnetic helicity fluxes, intervened in coronal mass ejections. At the moment there is no dynamo model seriously taking into account the magnetic helicity losses due to coronal mass ejections.

Distributed mean-field models assume dynamo action in the entire convection envelope. In the Sun, a shell $\alpha\Omega$-dynamo seems to be able to explain the 11-years sunspot cycle. The distributed dynamo models can produce the solar cycle just as well as flux-transport models, but the problem is how to generate sunspots from the mean-field. Solutions from various types of instabilities have been proposed, the most recent being the negative effective pressure instability (e.g. Brandenburg *et al.*, 2011a, and references therein). Based on the angular velocities of magnetic tracers, it is argued that the observations are compatible with a distributed dynamo that may be strongly shaped by the near-surface shear layer (e.g. Brandenburg, 2005, and references therein). If turbulent MHD models of flux rising in the convection zone will need a 10^5 G field, dynamo models and the location of the strongest fields need to be examined again. Which of the two dynamo scenarios is more real cannot be decided conclusively until more realistic turbulence simulations of the solar dynamo become available.

In convection-driven dynamo simulations made by Cole *et al.* (2014) the dynamo wave moved rigidly and was slower than the differentially rotating gas. The drift could not be explained by the differential rotation at any depth in the simulations. When rotation was rapid enough, the solutions were non-axisymmetric, like linear dynamo theory predicts. The non-axisymmetric mode, that was most easily excited, was of $m = 1$ type. This component also rotated rigidly at significantly different speed than the differential rotation of the surface. In rapidly rotating stars, however, the dynamo seems to work in a regime where the azimuthal dynamo wave and differential rotation have similar pattern speeds and these two mechanisms compete with each other (Cole *et al.*, 2014).

Oscillatory properties of dynamo types also play an important role in dynamo theory. The mean-fied $\alpha\Omega$-dynamo theory supports oscillating axisymmetric modes with a clear cyclic behaviour and sign changes, while α^2-dynamos with nonaxisymmetric solutions appeared to be in earlier studies quite steady, although nowadays oscillatory solutios also exist. There is a clear evidence that the differential rotation coefficient is decreased when the rotation increases, which suggest that the dynamos of these stars should indeed be of α^2-type. The dynamo theory does not rule out oscillating α^2-solutions and the origin of those are becoming somewhat more clear. Also, the disappearances and re-appearances of the non-axisymmetric dynamo waves remain without a direct explanation. It may be that the stellar magnetic fields consists both of axi- and non-axisymmetric components, the relative strength of which vary.

The discovery and identification of azimuthal dynamo waves from observations (see Chapter 5.1) acted as a driving force to pursue for producing models of rapid rotators with the full azimuthal extent. This research then led to a significant scientific breakthrough of their verification from DNS. Sudden phase jumps occur in observations, that are difficult to explain with two above mentioned scenarios. The sudden phase jumps, evidenced by many different observational methods, however, still remain somewhat enigmatic in terms of dynamo theory. The earlier reported flip-flops e.g. in II Peg, are not occuring in a cyclic manner indicating that flip-flops and magnetic cycles are not connected (e.g. Lindborg *et al.*, 2011; Hackman *et al.*, 2012, and references therein). The spot cycles are important phenomena in magnetic activity studies of stars. In this thesis we have clear evidence of spot cycles for both of our targets. To conclude, theoretically, it remains still unknown how sun- and starspots are formed, and in which layer the dynamo is operating. Thus great challenges still remain for both theoretical and observational studies.

Chapter 4

Optical observations of starspots

Starspots and activity cycles can be observationally studied in the optical wavelength region using photometric and spectroscopic techniques with proper observational facilities. While photometry can be done with small telescopes, spectroscopic monitoring is usually done using state-of-the-art instrumentation at medium-sized or large telescopes.

Regular monitoring of spotted stars began in the 1970's. Nowadays a great number of observations are done with Automatic Photometric Telescopes, which provide data through routine measurements of a high number of stars every night, weather conditions allowing. Space based photometry, e.g. COROT, MOST and Kepler, provides better accuracy and possibility to continuously observe targets, but the length of the observations are typically too short. Furthermore, the data are trend-corrected because of the systematic errors, which means problems in detecting long-term evolution such as stellar activity cycles.

Spectroscopy means the dispersion of light according to its wavelenghts and enables tracing individual spectral lines. Spectroscopy is responsible for providing almost all the knowledge we have about the physical properties of stars. Starspot studies require high-resolution spectrographs with high-sensitivity detectors. Inhomogenous structures like dark starspots on the stellar surface create distortions in the local spectral lines. When the star is rotating, these distortions move across the spectral line profiles. This effect is easily observed when the spectral lines are broadened by fast rotation.

The most direct way to detect stellar magnetic fields is to use spectropolarimetric techniques. Polarimetric observations of other stars than the Sun are challenging, because of the limited instrumental capabilities and due to disk-integrated observations of the Stokes parameters. Disk-integrated observations cancel the signal from regions of mixed polarity fields, and thus allows only for detecting large-scale magnetic fields. The weak spectropolarimetric signals from stellar magnetic activity require large collecting areas of telescopes or long exposure times.

4.1 Modeling of photometry

Since the discovery of cool spots causing photometric variations, three approaches have been commonly used to model those variations and to examine starspot properties: direct light curve modeling, light curve inversion and time-series analysis. Direct light curve modeling assumes a number of circular or other pre-defined shaped spots causing the variations. Numerical methods using these techniques were published by e.g. Budding (1977), Vogt (1981a), Rodonò *et al.* (1986) and Dorren (1987). A technique where the time-evolution of the spots is included was developed by Strassmeier and Bopp (1992). The pre-defined models are problematic, because they have a large amount of free parameters, and the spot shapes and distributions have to be assumed. To avoid these assumptions photometric light curve inversions have been developed (e.g Messina *et al.*, 1999; Berdyugina, 2002). Because the light curve is a one-dimensional time series, the derived stellar image contains information on the spot distribution mainly in the longitudinal direction, while spot extents and locations in latitudes stay uncertain. Thus the maximum spot concentration usually shows up at the central latitude of the stellar disk. Inversion or modeling the light curve is less informative than techniques that are based on spectroscopic observations, but long time-series of photometric data give us useful information on longitudinal spot patterns and their long-term evolution.

4.2 Photometric time-series analysis

By time-series analysis of photometry one can retrieve the period, amplitude, mean brightness and times of minima of the light curve. The photometric period is important for determining the rotation and differential rotation of active stars. The relation between the mean brightness and amplitude provides a method to find out how axisymmetrically spots are distributed. The spot coverage factor can be deduced from the mean brightness level. One can derive the longitudinal location or rotational phase of the spots from the photometric minima. Time series analysis of stellar photometry thus provides important parameters for examining long- and short-term changes of spot activity. In time series analysis spot models are not used.

The commonly used method for period analysis is the Fourier spectrum analysis. However, astronomical data are often too complicated for a straightforward Fourier analysis, because the observed light curves and spectra usually contain long time gaps caused by the observability of the targets and seasonal changes at the telescope site. This makes the analysis difficult and creates false peaks due to the regularities in the gap structure of the input data (see e.g. the review by Schwarzenberg-Czerny, 2003, and references therein).

TSPA (Three stage period analysis) is one of the more sophisticated methods applying harmonic decomposition to study stellar photometry (Jetsu and Pelt, 1999). A truncated Fourier series

$$g(t) = M + \sum_{k=1}^{K} B_k \cos(k2\pi ft) + C_k \sin(k2\pi ft) \tag{4.1}$$

is used as a periodic light curve model. The parameter M, the coefficients B_k, C_k and the frequency f are the free parameters and the parameter K is the highest Fourier mode to be fitted. The free parameters can be determined by a non-linear least-squares fit.

The light curves of active stars often have different modes of behaviour. They can be regular, periodic, or exhibiting relatively fast changes (Pelt *et al.*, 2011). The light curves are often described using simple trigonometric models, that rely on the assumption that the model parameters are constant in time. To cope with this Pelt *et al.* (2011) developed the carrier fit (CF) method, which is used in this thesis. The CF analysis is based on a straightforward decomposition of the light curve into two separate components: a rapidly changing carrier that traces the regular part of the signal, and its slowly changing modulation. The carrier frequency can be obtained from simple time-series analysis of photometric observations. The smooth modulation curves can be described by trigonometric polynomials or splines. Spline construction is better suited for stellar light curves with sharp phase jumps, while trigonometric polynomials can be used when relatively smooth changes are seen. The carrier fit method has been succesfully used for analyzing the phase changes seen in the light curve of FK Com (Hackman *et al.*, 2013) and II Peg (Lindborg *et al.*, 2013).

The proposed composition of the light curve is described with the following model:

$$f(t) = a_0(t) + \Sigma_{k=1}^{K}(a_k(t)\cos(2\pi tk\nu_0) + b_k(t)\sin(2\pi tk\nu_0)), \tag{4.2}$$

where ν_0 is the carrier frequency, $a_0(t)$ is the time-dependent mean level of the signal, K is the total number of harmonics included in the model, describing the overtones of the basic carrier frequency, while $a_k(t)$ and $b_k(t)$ are the low-frequency signal components. For synchronized binaries the first guess of the carrier frequency $\nu_0 = P_0^{-1}$ can be the inverse of the orbital period, while for other stars P_0 can be determined by e.g. a Fourier spectrum analysis of a limited part of the data. In some cases, such as for binary stars with orbital synchronization, a priori information of the carrier exists. In other cases, the carrier frequency can also be estimated through an optimization procedure (Pelt *et al.*, 2011).

In formulating the trigonometric modulator model, we use the full time span of the input data $[t_{\min}, t_{\max}]$. The data period is $D = C \times (t_{\max} - t_{\min})$, where C is a so-called coverage factor, the value of which must be larger than unity. The truncated

trigonometric series can be constructed by using the corresponding data frequency, $\nu_D = 1/D$, that is,

$$a(t) = c_0^a + \sum_{l=1}^{L} \left(c_l^a \cos(2\pi t l \nu_D) + s_l^a \sin(2\pi t l \nu_D) \right), \tag{4.3}$$

and

$$b(t) = c_0^b + \sum_{l=1}^{L} \left(c_l^b \cos(2\pi t l \nu_D) + s_l^b \sin(2\pi t l \nu_D) \right), \tag{4.4}$$

where L is the total number of harmonics used in the modulator model. The process described by the modulators and data period D must be slow. D must be significantly longer than the carrier period P_0.

The right estimates for the expansion coefficients must be computed for every term in the series for the fixed carrier frequency ν_0 and D; this is a standard linear estimation procedure and can be implemented using any standard statistical method (see Pelt *et al.*, 2011, for a detailed description). If all coefficients (a_k, b_k) consist of the same number of harmonics L and separate cycles are approximated by a K-harmonic model, then the overall count of linear parameters to be fitted is $N = (2 \times L+1) \times (2 \times K+1)$. The optimal number of harmonics, K, depends on the complexity of the light curve. The choice of the optimal number of modulator harmonics, L, is constrained by the longest gaps in the time series and the number of data points.

The exact error estimates and significance levels for the estimated mean periods can be computed by using either standard regression techniques, Monte Carlo type methods, the Fischer randomization technique, or bootstrap (Lindborg *et al.*, 2013). However, the real scatter of the mean period depends on the physics involved, and to estimate e.g. differential rotation, significantly longer data sets are needed, than the ones that are often available.

In Chapter 5 the results of the CF analysis of II Peg (Lindborg *et al.*, 2013) are compared with the temperature maps of II Peg (Lindborg *et al.*, 2011; Hackman *et al.*, 2011) and it is hence proved that observational methods can be useful in verifying and/or ruling out some theoretical scenarios arising from dynamo or differential rotation theories.

4.3 Doppler imaging

Doppler imaging (DI) is one of the most efficient observational techniques to examine stellar surface structures. DI techniques can be used both for mapping of temperature distributions in active late-type stars, as well as inhomogenities in element abundances in chemically peculiar stars. The main idea in DI is to use high-resolution spectral line profiles of rapidly rotating stars and invert them to surface maps.

Starspots create rotationally modulated distortions in the absorption line profiles of the stars, where the dominant broadening mechanism is rotation, and tracking these distortions, the temperature distribution on the surface of the target can be derived. The spot longitudes can be seen from the rotation phase when the bump is at the center wavelength of the spectral line, and the latitude can be deduced using the amplitude in Doppler shifts and the visibility of the bump. If the spot is at a low latitude, the bump moves all the way from the blue wing of the spectral line to the red wing when the star rotates. If the spot is at the visible pole, a constant deformation at the central part of the spectral line shape occurs. Vogt *et al.* (1987) introduced the DI technique for temperature mapping and since then it has been used successfully for a large amount rapidly rotating stars (e.g. Strassmeier, 2009, and references therein).

4.3.1 Regularization

The Doppler imaging problem can be formulated as searching for a surface temperature distribution X of the star that best reconstructs the observations. The discrepancy function to be minimized is

$$D(X) = \sum_{\phi_{\mathrm{sp},\lambda}} \omega_{\phi_{\mathrm{sp},\lambda}} \frac{(r_{\phi_{\mathrm{sp}}}(\lambda) - r^{\mathrm{obs}}_{\phi_{\mathrm{sp}}}(\lambda))^2}{N_{\phi_{\mathrm{sp}}} N_\lambda}, \tag{4.5}$$

where ϕ_{sp} is the rotation phase of the spectral observation, $N_{\phi_{\mathrm{sp}}}$ is the number of observed rotation phases in spectroscopy, N_λ is the number of wavelength points in each spectrum, and $\omega_{\phi_{\mathrm{sp},\lambda}}$ is the weight of each point. The normalized spectral profiles $r_{\mathrm{sp}}(\lambda)$ are calculated for a given surface distribution X, and compared to the observations $r^{\mathrm{obs}}_{\phi_{\mathrm{sp}}}(\lambda)$.

The discrepancy D is in a way an operator over X and the solution could be reached by constructing the inverse operator D^{-1}. The problem is, however, ill-posed, as small perturbations in the data will lead to very different solutions. To stabilize the ill-posed inverse problem, additional information can be added as structure constraints (Goncharskii *et al.*, 1977, 1982).

The DI technique used in this work is based on the method called Tikhonov regularisation. Generally this means introducing an additional structure constraint minimizing the surface gradient of the solution. Also other alternative techniques exist, the most famous of them being Maximum entropy method (Vogt *et al.*, 1987) and Occamian approach (e.g. Berdyugina, 2005). The choice of method should not significantly change the solution, as long as the quality of the data is good.

In Tikhonov regularisation the problem to be solved is formulated so, that the quantity $\Phi(X)$ to be minimized is

$$\Phi(X) = D(X) + \Lambda R(X), \tag{4.6}$$

where Λ is a Lagrangian multiplier and

$$R(X) = \int\int \|\nabla X\|^2 d\sigma \tag{4.7}$$

is the Tikhonov regularisation function, where $d\sigma$ is the surface element and $\|\cdot\|$ is the Euclidean norm describing the system being potentially under- or overdetermined. The regularisation function describes the smoothness of X, and the method aims at searching for the smoothest solution that reproduces the observations (Piskunov *et al.*, 1990). The discrepancy $D(X)$ should ideally correspond to the observational errors and the parameter Λ should be adjusted so that the noise in the observations is not modeled.

4.3.2 Requirements

The DI technique has limitations for its usage. In order to get a trustworthy Doppler image of a star, several conditions have to be met. The star must be a fast rotator, having a minimum value $v \sin i$ of around $20 - 30$km/s, in order to have sufficient spectral line broadening due to rotation, and to thus get a useful amount of resolution elements. The larger the $v \sin i$, the better resolution that can be obtained (Vogt *et al.*, 1987), but too large $v \sin i$ results in too wide lines and the features in the profile become blurred due to line blending.

The stellar inclination i should roughly fall into the range of 30 to 70 degrees. If i is close to zero degrees, there is no line-of-sight velocity components. If i reaches 90 degrees, it is impossible to see on which hemisphere a surface feature is, so this results in a mirror-image symmetry around the stellar equator. For large inclinations (i is more than 70 degrees), the mirroring effect is always a problem (Vogt *et al.*, 1987). Also a high signal-to-noise ratio (at least S/N=200) of the observations is needed to measure the distortions in the line profiles as well as a high spectral resolution. When observing with smaller telescopes or faint targets with short periods, the S/N might cause a problem, because the stellar rotation phase changes during the exposure and image resolution is thus lost. A low S/N ratio may be compensated by modeling many spectral lines or using techniques such as the least squares deconvolution (LSD) Donati *et al.* (1997). A minimum of around 10 spectra evenly distributed over the rotation phases are needed for a reliable Doppler image. In some cases the spot distribution might have changed before a sufficient phase coverage is reached.

4.3.3 Stellar and spectral parameters

The stellar parameters needed for DI are element abundances, microturbulence, macroturbulence, gravity, rotation velocity, inclination of the rotation axis and rotation period. The choice of parameters used is not trivial, because different parameters

have similar effects on the spectral lines, and appropriate fits can be obtained by using different combinations of stellar and spectral parameters. The inversion procedure is very sensitive to changes in the microturbulence; varying it shifts the average effective temperature $T_{\rm eff}$ of the solution. An inaccurate $v \sin i$ can produce artefacts seen as polar caps, and hot or cool belts in the Doppler imaging maps. Thus, establishing the connection between the variation on the stellar parameters and the resulting line profiles is crucial (e.g. Lindborg *et al.*, 2011; Hackman *et al.*, 2012).

Setting the stellar parameters for single stars like DI Psc (Chapter 6) is more demanding than for close binaries (Chapter 5). In the latter case the inclination can be deduced from the orientation of the binary orbits, while in the former case the inclination is often roughly estimated from known rotation periods, the $v \sin i$, and an assumed radius. Vogt *et al.* (e.g. 1987) made tests how different (wrongly chosen) inclinations influence the Doppler imaging result. Their conclusion was, that the overall locations of spots and shapes of spots are well preserved and insensitive to errors.

The spectral line parameters used in DI are the central wavelength, excitation potential, $\log gf$ value, and damping parameters. These values can be adopted from catalogues or databases, e.g. the Vienna Atomic Line Database (Kupka *et al.*, 1999). The uncertainties in both stellar and spectral parameters can be solved by testing a wide range of values and selecting the set of parameters, which produces the minimum discrepancy and the fastest convergence of the inversion (e.g. Rice, 2002). If there are several unknown parameters, the inversion process is iterative.

4.3.4 Temperature imaging step-by-step

In this thesis we use the inversion method called INVERS7, which was developed by N.E. Piskunov (Piskunov *et al.*, 1990; Piskunov, 1991). The DI solution is retrieved using a table of calculated local line profiles for different surface positions (limb angles) and different effective temperatures. The first part of the procedure is to compute a table of local line profiles for a sequence of model atmospheres with different effective temperatures. This is also the most demanding part in DI. For this we need a set of stellar and spectral parameters. The local spectral line and continuum intensities are calculated using the radiative transfer equation and numerical model atmospheres. The convolution of the local line profiles with the Gaussian instrumental profile and radial/tangential macroturbulence can be done after this. Then the synthetic spectral profile is calculated using a given surface temperature map enabling the search for the best solution.

The grid of the model contains a limited range of effective temperatures. To avoid extrapolation, a penalty function $F_p(X)$ can be added to the function to be minimized

to limit the model atmospheres to $[T_{\min}, T_{\max}]$ in the form

$$F_p(X) = \sum_i f_p(T_i), \tag{4.8}$$

where T_i is the temperature of the surface element and $f_p(T_i)$ is 0, when $T_i \in [T_{\min}, T_{\max}]$. If $T_i \notin [T_{\min}, T_{\max}]$, $f_p(T_i)$ can grow linearly (Hackman, 2004). The easiest way is to use a function defined in intervals. In this thesis we apply the following function. We define x_T as

$$x_T = \frac{2T_i - (T_{\max} + T_{\min})}{(T_{\max} - T_{\min})}. \tag{4.9}$$

The penalty function can then be formulated as

$$f_p(x_T) = \begin{cases} 0, & |x_T| \leq 1 \\ 1 - \sqrt{1 - (|x_T| - 1)^2}, & 1 < |x_T| < 1 + \frac{\sqrt{2}}{2} \\ |x_T| - \sqrt{2}, & |x_T| \geq 1 + \frac{\sqrt{2}}{2}. \end{cases} \tag{4.10}$$

The minimisation procedure in INVERS7 is based on a conjugate gradient algorithm. Usually 30 iterations is enough to achieve an optimal solution.

4.4 Zeeman-Doppler imaging

The cool spots detected by photometry and DI are usually interpreted as being generated by strong magnetic fields decreasing the plasma flow velocity, which is true for the solar case. The Sun used to be the only late-type star, for which surface magnetic fields could be mapped. It is, however, known that the level of magnetic activity, magnetic field strength and configuration change from a different type of late-type star to another. To be able to understand how dynamos operate in different kind of late-type stars, we need observational information on how well the sunspot analogy works, how large the starspots actually are, and how the large-scale magnetic field is distributed on the stellar surface.

The availability of high-resolution spectropolarimetry has opened a new era for Doppler imaging. Rotationally modulated distortions caused by surface magnetic fields are often observed only in the Stokes V parameter, but sometimes also in Stokes U & Q (Rosén *et al.*, 2013). In Zeeman-Doppler imaging (ZDI) Stokes I,V,Q and U spectra can be used to map surface magnetic fields of stars (Semel, 1989; Brown *et al.*, 1991). The main problem is that the weak signal even in Stokes V (circular polarization) means very high S/N observations are needed. By combining multi-line spectropolarimetric observations through least-squares deconvolution (LSD), the S/N of spectropolarimetric observations can be enhanced enough for mapping the surface magnetic field of late-type stars (Donati *et al.*, 1997). The LSD-method combined

with ZDI has successfully been applied to a number of stars, revealing both the topology and evolution of the surface magnetic field (see e.g. Petit *et al.* (2004, 2009); Kochukhov *et al.* (2013)).

A common interpretation problem of ZDI maps is that the polarization signature of surface structures appears to be stronger outside cool starspots. Most of the ZDI codes keep temperature and magnetic inversions separate, but the reconstruction of magnetic field is improved when local temperature variations are taken in account (Rosén and Kochukhov, 2012). ZDI can provide spatially resolved information about stellar magnetic field topologies and fine details of field geometries (Kochukhov *et al.*, 2013), but so far the majority of ZDI studies of cool stars neglect the effects of temperature spots in the magnetic field inversions (Rosén and Kochukhov, 2012). Recently, a new line profile reconstruction technique based on a singular value decomposition (SVD) was used by Carroll *et al.* (2012). They obtained a magnetic field structure which showed a good spatial correlation with the surface temperature, and was dominated by a strong field within the cool polar spot.

The main problem with ZDI is that the measured magnetic field is weighted by the flux. This means a strong field in a cool spot may be undetected, while a weaker mean field is measurable. Furthermore, the usage of just Stokes I & V may be problematic as different magnetic field structures may produce similar Stokes V signals (e.g. Kochukhov *et al.*, 2010). ZDI would certainly benefit from studies using the same observations but different ZDI codes. Meanwhile, temperature imaging presently appears to be more trustworthy.

Chapter 5

Analysis of II Pegasi

Rapidly rotating active late-type stars are usually either young objects or close binaries. RS CVn stars form a system of close detached binaries with strong photometric variability (Eaton and Hall, 1979). The spot coverage can be even half of the visible hemisphere, which makes these binaries interesting targets for Doppler imaging. RS CVn stars typically have strong chromospheric Ca II and H&K emission lines and orbital periods of a few days up to 30 days. They also show optical variability that can be characterized by an amplitude of up to 0.6 mag in the V-band, and interpreted as a rotation-modulated effect of cool spots. Hall (1976) proposed the following classification signatures to type RS CVn stars: photospheric variability, Ca II H&K emission lines, subgiant component within its Roche lobe, and fast rotation meaning almost synchronized rotation of the components with respect to the orbital motion of the binary system.

II Pegasi (HD 224085) is one of the most active and best studied RS CVn stars with a rotation period of roughly 6.7 days. The primary component of II Peg is a K2 subgiant of luminosity class IV (Berdyugina *et al.*, 1998a). Because of the low luminosity of the secondary component, II Peg appears as a single-line binary, thereby making its spectral analysis easier.

Vogt (1981b) was the first to try to reconstruct magnetic fields of II Peg. He derived starspot areas from photometric and spectroscopic observations in 1977-1978, and estimated the longitudinal magnetic field during different rotation phases. The first surface temperature maps were calculated by Hatzes (1993), followed by photometric light curve variation analysis by Berdyugina and Tuominen (1998) and Rodonò (2000). The results of Berdyugina and Tuominen (1998) and Berdyugina *et al.* (1998b, 1999b,c) were reported to be consistent with a spot configuration concentrated on two active longitudes separated approximately by 180 degrees. The system of active longitudes was migrating in the orbital frame of reference, and the photometric and spectroscopic time series available at that time were indicating a regular switch of activity level between the longitudes, with a period of about 4.65 years. In the sur-

face images of Gu *et al.* (2003), the general spot pattern was quite similar, but the drift with respect of the orbital frame was less obvious, and the switch in the activity level was reported to occur earlier than predicted by Berdyugina *et al.* (1999b). Rodonò (2000) found a much more complicated spot pattern from their photometric study: the existence of a longitudinally uniformly distributed component was reported, showing three active longitudes, with a 13.5 years cycle. Xiang *et al.* (2014) published two Doppler images for February and November 2004 showing both high-latitude and equatorial bands of spot activity, no preferred active longitudes, and significant changes in the spot distribution during time scale of nine months. X-ray flares on II Peg were first detected in the mid-1970's (Schwartz *et al.*, 1981) and later on flare activity on II Peg has been reported several times (e.g. Berdyugina *et al.*, 1999a; Siwak *et al.*, 2010). The surface patterns might change, including positions of active regions, during optical flare events. Donati *et al.* (1992) made the first Stokes V measurements for the star, in order to use them for Zeeman-Doppler imaging, but no surface magnetic field maps were published at that time. Later on ZDI maps have been published of the target (e.g. Carroll *et al.*, 2009; Kochukhov *et al.*, 2013). So far no clear connection between cool spots and magnetic structures have been confirmed.

We have studied the spot activity of II Peg during the years 1994-2010 with Doppler imaging and completed the analysis with a carrier fit analysis of photometry. The spectral observations were collected with the Nordic Optical Telescope. The photometric observations consist of several separate datasets covering as long time span as possible (Lindborg *et al.*, 2013, and references therein). In total 28 images were calculated for the years 1994-2010 (Lindborg *et al.*, 2011; Hackman *et al.*, 2012). As a result, we found that the surface of the star was dominated by one single active longitude that was drifting in the rotational frame of the binary system during 1994-2002. The spot generating structure seemed to be rotating somewhat more rapidly than the binary system. This drift was particularly evident during the years 1997-1999. The drift was first reported by Lindborg *et al.* (2011), but it was also visible in the results published by Berdyugina and Tuominen (1998). Later images for 2004-2010 showed decreased and chaotic spot activity, with no signs of the drift pattern. It seems that II Peg entered a state of weaker activity and magnetic field strength than during 1994-2002, and this could be related to a minimum in the star's magnetic cycle, and no clear trace of the drift is visible in ZDI maps published by Kochukhov *et al.* (2013). Also the magnetic field seemed to become more axisymmetric during the minimum.

We combined all collected V-magnitude photometric data into one single data set to study the drift, and analysed it with the CF method. We confirmed that the spot activity has been dominated by one active region almost through the entire data set

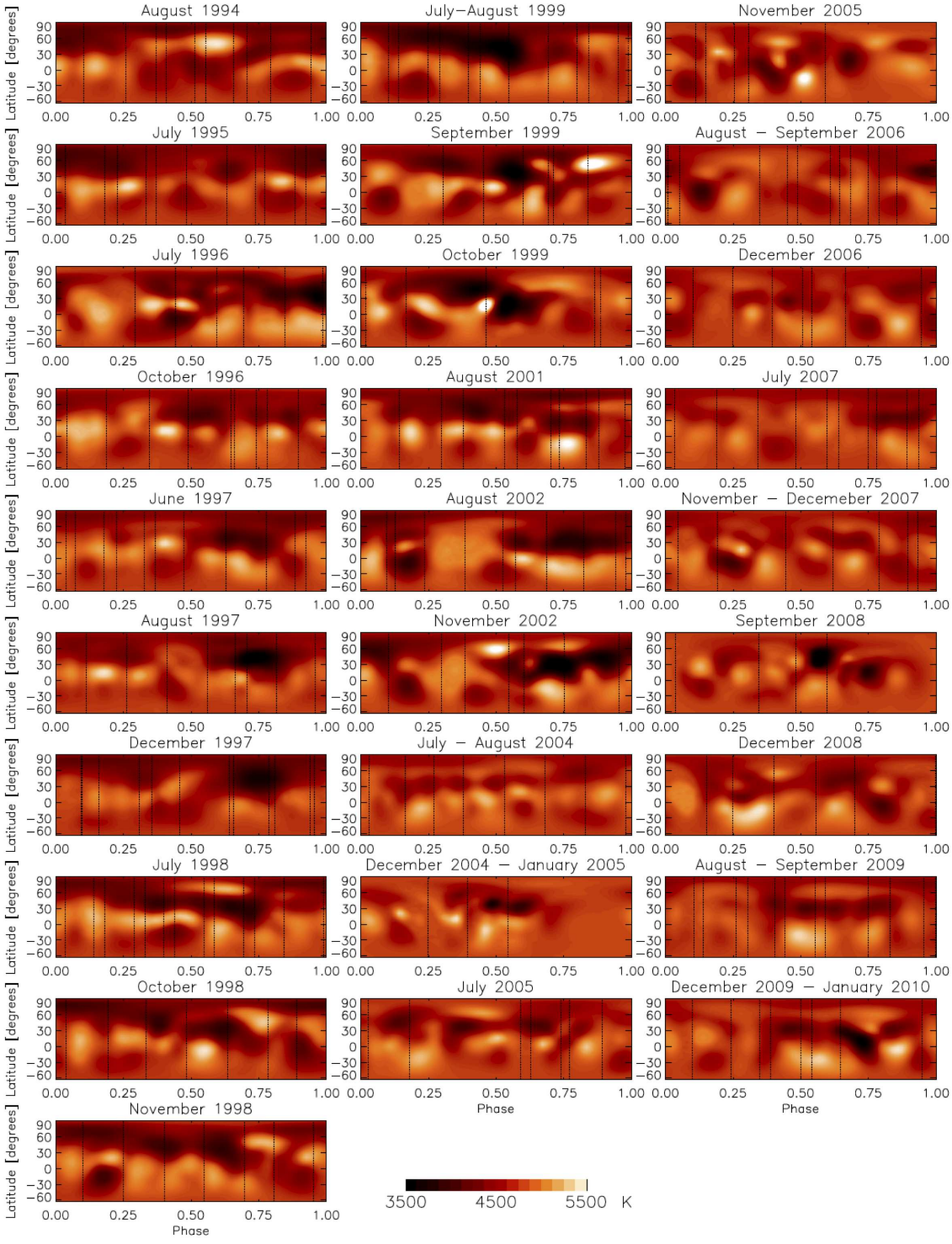

Figure 5.1: Doppler images of II Peg for 1994-2010. The figure shows equirectangular projections of the obtained surface temperature distribution. (Figure adopted from Hackman *et al.* (2011))

associated with a nearly linear drift. Complicated phase behaviour and a break of the linear trend were also seen, but the period analysis revealed a rather stable periodicity. After removing the linear trend from the data, several sudden phase jumps occurred, three of which we analysed more carefully with the CF method. These phase jumps looked like the reported flip-flop events, but the new spot configurations did not persist longer than a few months, which would not fulfil the flip-flop criteria (e.g. Kajatkari *et al.*, 2014). Moreover, the flip-flops did not occur periodically. The regular drift without phase jumps was related to the high activity state, while the complex phase behaviour and disrupted drift pattern to the low activity state by comparing photometric results to the ones from DI and ZDI.

The drift behaviour seen in II Peg during the years 1994-2002 could in principal have three different birth mechanisms: the star is not yet synchronized, differential rotation, or an azimuthal dynamo wave. As the star is in a binary system, the binarity itself could enhance the non-axisymmetric dynamo modes, as has been proposed, e.g., by Moss *et al.* (1991) and Holzwarth and Schüssler (2003). Binarity-induced non-axisymmetric modes would, on the other hand, be synchronized to the orbital motion of the binary system, as the tidal effects are thought to influence the dynamo via persistent non-axisymmetricities in the turbulent quantities. Therefore, binary-induced modes would most likely be stationary in the rotational frame of the binary system, contrary to what is actually deduced from observations. We set out to study if this drift is a persistent phenomenon, in which case it could be caused either by an azimuthal dynamo wave or be an indication that the binary system's orbital synchronization is still incomplete, although the facts that the drift is not observed all the time and the star is old do not support this latter scenario. The option that the differential rotation of spots at more or less fixed latitude positions could cause the persistent drift, should also be considered. Because the drift period is shorter than the orbital one, and the spots are persistently seen at high latitudes, one explanation for the drift could be a weak anti-solar (pole rotating faster than the equator) differential rotation.

Rapidly rotating late-type stars with deep convective envelopes are expected to exhibit very small differential rotation. For II Peg this has been confirmed from observations (Siwak *et al.*, 2010; Roettenbacher *et al.*, 2011). The amount of differential rotation between the orbital motion and that of the spot motions at their fixed, relatively high latitude can be estimated as (Lindborg *et al.*, 2013):

$$\mid k \mid = \frac{P_{\rm spot} - P_{\rm rot}}{P_{\rm rot}} \approx 0.002. \tag{5.1}$$

The estimated differential rotation is consistent with the values derived by Siwak *et al.* (2010), who assumed solar differential rotation, but higher than the value estimated

by Henry *et al.* (1995). Our method of estimating the differential rotation is based on the spots being fixed at certain latitudes as indicated by the Doppler images, when the other methods transform detectable period variations into differential rotation, attributing these changes to changing spot latitudes. Theoretical and numerical models predict a solar-like differential rotation patterns for rapid rotators (e.g. Cole *et al.*, 2014, and references therein). In this light, the antisolar rotation profile that our results would imply must be considered unlikely.

Dynamo waves are by theory expected to occur in rapidly rotating late-type stars (e.g. Krause and Rädler, 1980; Tuominen *et al.*, 2002). The disappearing wave can be explained by the evolution of a stellar magnetic cycle. Two migratory active longitudes are also an expected result in dynamo models. Our results inspired more theoretical investigations: Cole *et al.* (2014) studied rapidly rotating DNS models over the whole azimuthal extent, and the models excited large-scale $m = 1$ magnetic fields. Those fields rotated at different speeds than the fluid itself. Moreover, the differential rotation generated in the models did not affect those fields. The drift of the nonaxisymmetric mode in the DNS models resembles both the predictions of mean-field dynamo theory and the observed drift pattern of II Peg, although in the DNS models the dynamo wave had a longer period. Mode $m = 1$ and the drift are similar to what we got from the observations. The difference in the pattern speed of the nonaxisymmetric mode and surface rotation, however, is much higher than in the observations. The drift could not be explained by the differential rotation at any depth in the simulations, so that ruled out the differential rotation scenario and left the dynamo wave option the only possible solution for the drift. The most possible solution for the drift is thus a manifestation of an azimuthal dynamo wave observed on II Peg that later on vanished when the star entered to a decreased activity state, when the large-scale magnetic field of the star was also more axisymmetric.

Chapter 6

Analysis of DI Piscium

DI Piscium (HD 217352) is located at a distance of 190^{+30}_{-23} parsecs from the solar system (van Leeuwen, 2007), and is a low mass lithium-rich [LTE log n = 2.20] giant (Kővári *et al.*, 2013) with a rotation period of 18.4 days (Strassmeier *et al.*, 2000). The spectral type of DI Psc has been determined to be K1 III (e.g. Kővári *et al.*, 2013, and references therein). According to Gray (2008) this gives an effective temperature $T_{\text{eff}} \approx 4700K$, and a surface gravity $\log g \approx 3$.

Lithium in the universe is a hot topic in astronomy, because there is less of it in stars than the standard big bang nucleosynthesis would predict. Roughly 1% of post-main-sequence stars, however, have significantly more lithium than stellar evolution models predict. Lithium-rich K giant stars are located at the luminosity bump of the first ascending red giant branch. With stars of this type important connections can be studied, e.g. thermonuclear processes, rapid mixing, surface activity, rotation and mass loss episodes.

It has been postulated that the rare population of lithium-rich K-giants is composed of objects rotating faster than ordinary giants of the same type (e.g. Reddy and Lambert, 2005; Drake *et al.*, 2002). DI Psc is one of the fastest rotators within this population. Further studies are still needed to determine if the angular momentum of DI Psc is added to the envelope from the interior (rapidly rotating core), or from outside (merging planet), or if it is an effect of merged binaries (Drake *et al.*, 2002).

It is not clear what causes the anomalously high lithium abundances in this class of objects. Lithium is destroyed at a star's main sequence phase, and can mainly survive in a thin layer at the surface of the star due to the lack of mixing between this and other layers. There are some observational indications that rapidly rotating stars preserve lithium better than slower ones of the same mass and that the rotation hinders overshooting and lithium burning (e.g Tschäpe and Rüdiger, 2001, and references therein). Several observations of lithium abundances in K giants confirm that the values observed are close to the predicted upper limit (e.g. Melo *et al.*, 2005; Kumar *et al.*, 2011). In some objects the values can even reach the present interstellar

medium value (see e.g. de La Reza and da Silva, 1995; Balachandran *et al.*, 2000).

Charbonnel and Balachandran (2000) describe two methods for lithium production. Low-mass red giant branch stars, that have a helium flash, produce lithium at the phase seen as a bump in the luminosity function. When the outward moving hydrogen burning shell, due to the increasing helium core mass, first meets the convective envelope, the surface luminosity is decreased, because the availability of extra hydrogen decreases the mean molecular weight. The bump in the luminosity function is created in the slowing down phase in evolution time-scale of the giant's evolution (Iben, 1968). The outwardly moving hydrogen shell burns through the mean molecular weight discontinuity (Charbonnel and Balachandran, 2000) and extra mixing processes, like the one induced by rotation, can now connect the helium rich envelope material to the outer regions of the hydrogen burning shell, which activates lithium production. This can produce a higher lithium abundance, but the phase is very short-lived, because lithium is easily destroyed. Most of the lithium-rich K giants have luminosity and effective temperature combinations, that allow lithium production at a helium core flash, which has been proposed as another possible mechanism responsible for the lithium-rich giant population (see e.g. Kumar *et al.*, 2011).

The main cause of these abnormal abundances of lithium in low mass red giant stars still remains unknown (e.g. Kumar *et al.*, 2011), as none of the scenarios are directly supported by observational evidence. For instance, even though the lithium-rich red giant branch stars rotate faster than average, high lithium abundances have been observed in slow rotators, and low abundances in fast rotators, casting some doubt on the importance of the extra mixing provided by rotation.

Kővári *et al.* (2013) published the first temperature map of DI Psc for May 2000, which showed a high temperature contrast of around 1000 K with polar and belt-like spot structures. We wanted to extend this study. Our observations were taken at the Nordic Optical Telescope, between 2004-2006. The map of July-August 2004 (Fig. 6.1), which was our best observing season with high phase coverage, revealed a more or less spotless appearance with a temperature contrast of around 300 K. This was a significant change from the May 2000 surface temperature maps published by Kővári *et al.* (2013), showing large polar and belt-like low-latitude spot structures with a notable temperature contrast. Although the inversion method, and some adopted stellar parameters (such as the inclination) were different from ours, the observations were also of good quality with sufficient phase coverage. Both of the maps could be regarded almost equally reliable, and the differences are unlikely to be caused by the choise of method.

Our November 2005 and September 2006 images have rather low phase coverages. In November 2005, when we have only four observations, the case is worsened by a

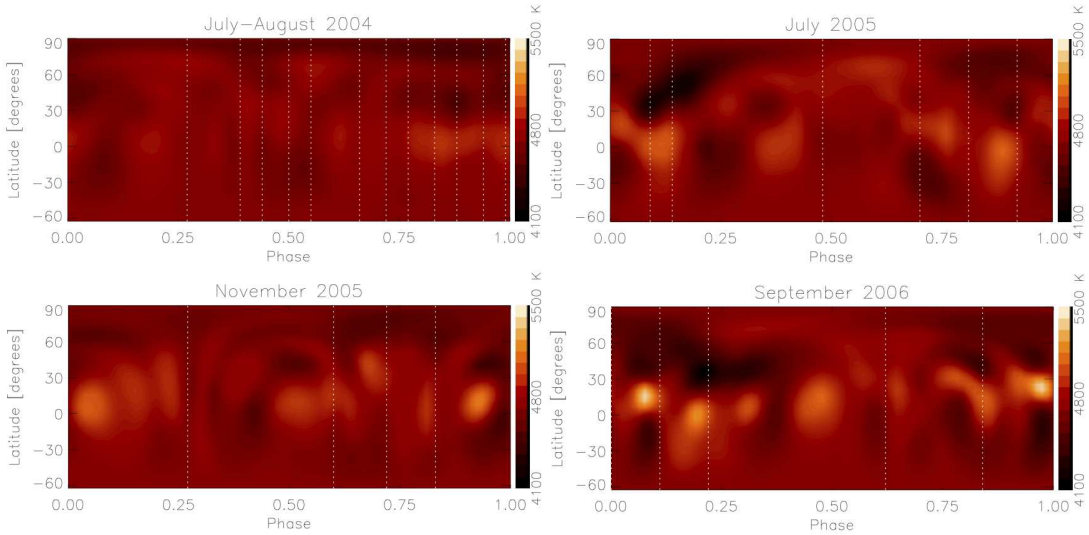

Figure 6.1: Doppler images of DI Psc in 2004-2006. The figure shows equirectangular projections of the obtained surface temperature distributions.

Table 6.1: Summary of average temperature, $T_{\rm mean}$ and temperature difference $\Delta T = T_{\rm mean} - T_{\rm min}$, spot filling factor F_S, and deviation (d) of the DI solution in the obtained inversion maps.

Season	$T_{\rm mean}$ [K]	ΔT [K]	F_S [%]	d [10^{-5}]
JulAug04	4690	270	0.0	6.19
Jul05	4700	553	21.3	5.52
Nov05	4700	330	1.4	5.13
Sep06	4690	590	35.2	5.56

quite low signal-to-noise ratio. Some spot structures are centred at phases where we do not have observations, so it is hard to say if those spots are real. However, the presence of spots is cleary seen from bumps in spectral lines in the observations from 2005 and 2006. The temperature contrasts were also rising from 2004, being around 550 K in July 2005, 330 in November 2005 and around 600 K in September 2006. Furthermore, as demonstrated by e.g. Vogt *et al.* (1987) and Rice and Strassmeier (2000), poor phase coverage mainly affects the positions and shapes of spots, but should not introduce completely spurious spot structures. We thus regard the spot filling factors as, if not completely accurate, at least qualitatively correct. Table 6.1 show the summary of of the inversions.

According to our surface temperature maps of DI Psc, the spot coverage fraction has varied strongly within a time scale of a few years. The strong spot activity

observed in May 2000 by Kővári *et al.* (2013) practically disappears within four years to July-August 2004. After this the spot activity regained some of its strength until July 2005. The November 2005 map shows weaker spot activity, but in September 2006 the activity is again stronger. Recently Kriskovics *et al.* (2013) presented new DI maps for November-December 2012 indicating a similar level of activity as in May 2000. The spot evolution of this kind can be a consequence of an activity cycle, but the follow-up time is too short for a conclusion on any periodicities in the activity level.

The convective turnover time, $\tau_{\rm c}$, of G–K giants in the luminosity classes III–IV can be estimated to be on average 50 d (see e.g. Saar and Brandenburg, 1999, Table 4, and references therein). The stars are not spread evenly in the diagnostic diagram (see Chapter 2; Fig. 2.6), but are forming populations. The diagnostic diagram in Fig. 2.6 shows active (A) and superactive (S) branches of stars as well as an inactive (I) branch. This diagram can be used to predict the length of the magnetic cycle, when the rotation rate is known. Using the rough estimate of $\tau_{\rm c}$, would give Co $\equiv 4\pi {\rm Ro}^{-1} \equiv 4\pi\tau_{\rm c} P_{\rm rot}^{-1} \approx$35 for DI Psc. This places DI Psc at the high-Coriolis number edge on the 'active' branch of the diagnostic diagram on which stars systematically show magnetic cycles of the order of a few hundred times the rotational period, i.e. a few years to ten years. On this branch, the magnetic activity cycle length decreases as a function of the rotation rate. The relatively large variations seen in the spot coverage fraction during only a few years can at least be considered to rule out the possibility of DI Psc exhibiting a very long magnetic cycle characteristic for the 'superactive' branch or stars transiting towards it. The observational data collected so far is however, not long enough to distinguish whether the star belongs to the 'active' or the 'inactive' branch.

Chapter 7

Conclusions

Recent years have shown a number of important advances both in the modeling and observational frontiers of studying active late-type stars. In the former, the first solar-like dynamo solutions have been obtained from direct numerical simulations (e.g. Käpylä *et al.*, 2012). Moreover, inspired by the observational studies such as the ones presented here, direct numerical simulation (DNS) models of rapid rotators have been performed (e.g. Cole *et al.*, 2014), resulting in the confirmation of azimuthal dynamo waves that have different rotational velocities than the stellar surface. In the latter frontier, the photometric, spectroscopic and spectropolarimetric time series collected start to reach time extents from which it is becoming possible to detect stellar magnetic activity cycles. Mean-field dynamo models can produce many observed features both of the solar cycle and some of the features seen in active rapid rotators, but it remains yet under debate which one of the dynamo paradigms (flux transport, distributed dynamo) is correct. Especially in the case of the Sun, the kinematic mean-field models of either type can lead to a satisfactory reproduction of the solar cycle main properties. The photometric, spectroscopic and spectropolarimetric observations help us to draw conclusions on the type of the dynamo modes in other stars than the Sun, which, in turn, helps us to better understand the solar dynamo itself.

The Doppler imaging technique provides us with essential information about the spot activity, variations of the spot coverage, spot configuration and evolution of active regions. Furthermore differential rotation can be estimated with DI (see e.g. Petit *et al.* (2004)). The rapidly rotating stars II Pegasi and DI Piscium in this study are highly active compared to the Sun, but may still have similarities with the young Sun, which also rotated fast.

II Peg has been spectroscopically monitored for nearly 20 years, so we have a quite clear image what happens in the star during that time-span. The surface of the star was dominated by one single active longitude that was drifting in the rotational frame of the binary system during 1994-2002 (Lindborg *et al.*, 2011; Hackman *et al.*,

2011). We interpret this drift as a manifestation of an azimuthal dynamo wave. Later imaging for 2004-2010 showed decreased and chaotic spot activity with no signs of the drift pattern (Hackman *et al.*, 2012). It seemed that II Peg entered a state of weaker activity after the year 2002, and this could have been related to a minimum in the star's magnetic cycle. From the ZDI study of Kochukhov *et al.* (2013) this seems likely, as the magnetic field of the object was measured to be weaker during that epoch. Moreover, the magnetic field appeared to be more axisymmetric during the minimum. We also investigated the possibility of a weak differential rotation as a probable source for this drift (Lindborg *et al.*, 2013). Both the predicted length of the magnetic activity cycle and the amount of differential rotation still fell in sensible ranges. However, as the DI showed the latitudes of the spots being concentrared at high latitudes, and the latitudes of spots being roughly constant over time, the faster rotation of the spot structure derived from photometry would necessarily imply anti-solar differential rotation. Such differential rotation is not consistent with results from numerical modeling of rapidly rotating late-type stars (e.g. Käpylä *et al.*, 2011a,b; Gastine *et al.*, 2014; Brun and Palacios, 2009), which predict solar-type rotation laws (fast equator, slow poles) for rotation rates higher than the Sun. The observational studies inspired numerical modeling made by Cole *et al.* (2014). This study proved the differential rotation scenario unlikely and supported the dynamo wave being the most probable source of this drift.

DI Psc is an extremely interesting rapid rotator due to its high lithium abundance. According to all produced surface temperature maps of DI Psc, the spot coverage fraction has varied strongly with a time scale of a few years. The strong spot activity observed in May 2000 by Kővári *et al.* (2013) practically vanished within the four years to July-August 2004. After this, according to the maps we computed (Lindborg *et al.*, 2014), the spot activity regained some of its strength until September 2006. The spot evolution of this kind can be a consequence of an activity cycle, but the follow-up time is too short for conclusion on any periodicities in the activity level. Therefore it would be interesting to continue the observations of the star for longer time-spans to get a confirmation if the star really has a short few years activity cycle.

The images from the Sun show the spot sizes and shapes clearly, but from Doppler images it is not so easy to determine the sizes and areas, because the images appear smoother and are of poor resolution. The smoothness can be real, but also an artefact, because of the choice of the regularization algorithm. The spots are most likely constantly changing like in the Sun, so it would be good to analyze the same star with better time resolution and more continuously. It would also be interesting to investigate the coronal activity of II Peg and DI Psc and see the correlation between the corona and the photospheric activity. This would demand more coordinated

groundbased and satellite observations, such as those reported by Doyle *et al.* (1992) and Byrne *et al.* (1998).

MHD simulations of sunspots might give us a tool to explain the starspots and their birth mechanisms. New global MHD models are needed to explain the huge starspot sizes and long life-times of them. A physically consistent dynamo model should take into account the interfaces in the tachocline at the bottom of the convection zone that interacts with the core, and the stellar surface that acts as the interface to the exterior. The tachocline most likely dominates the magnetic field generation by the dynamo in solar-type stars, while the surface layer connects the atmosphere and back-reacts on the outer layers of the convective envelope. The surface layers might also be important for the dynamo both by providing helicity fluxes that prevent the dynamo from suffocating to its own waste product and because dynamo efficiency is increased by the surface shear layer, which also can facilitate the correct migration direction of the latitudinal dynamo wave.

The connection between cool spots and magnetic fields in the Sun has seldom been detected in other stars and it is not yet obvious that this relation can be extended to other types of cool active stars besides of the Sun. A completely different scenario for the origin of the cool spots of rapidly rotating stars has been studied by Käpylä *et al.* (2011c) and Mantere *et al.* (2011), who proposed that the formation of temperature anomalies on the surfaces of rapidly rotating late-type stars could be generated due to the hydrodynamical instability creating large-scale vortices. This could also give another explanation for the hot spots near the large cool spots detected in several rapidly rotating stars, including DI Psc and II Peg in this study, by Doppler imaging: These may not be artefacts, but actually a real phenomenon.

It is nowadays possible to model the observed phenomena with efficient numerical models, and thus combining the observations with the theory. Many open questions still remain unanswered: Are starspots analogues to sunspots, and are large starspots singular spots or spot groups? Do starspots have simple or mixed magnetic polarity? Could vortices at the stellar surface cause temperature variations?

Chapter 8

Publications

The summaries of the five included articles are given here. The contribution of the author of this dissertation to the articles is included at the end of each summary.

Paper I

Lindborg, M.; Korpi, M. J.; Hackman, T.; Tuominen, I.; Ilyin, I.; Piskunov, N.: Doppler images of the RS CVn binary II Pegasi during the years 1994-2002, Astronomy & Astrophysics, Volume 526, A44, 7p, 2011.

We published 16 new Doppler imaging temperature maps for the years 1994-2002. The derived temperature maps were quite similar to the ones obtained earlier with different methods and the main differences occurred in the spot latitudes and relative strength of the spot structures. The surface of the star was dominated by one single active longitude that was drifting in the rotational frame of the binary system during 1994-2002. This drift was particularly evident during the years 1997-1999 and was first discovered in this paper. The observed drift of the spot structure in II Peg can be explained by an azimuthal dynamo wave and thus would be one of the first observed dynamo waves of this kind.

The main author had the responsibility of spot modeling, analysis of the results and writing of the paper. The analysis of the publication was heavily influenced by the discussions about the dynamo theory and observational viewpoint of it with Maarit Mantere and Thomas Hackman.

Paper II

Hackman, T.; Mantere, M. J.; **Lindborg, M.**; Ilyin, I.; Kochukhov, O.; Piskunov, N.; Tuominen, I.: Doppler images of II Pegasi for 2004-2010, Astronomy & Astrophysics, Volume 538, A126, 8p, 2012.

We continued to study the spot activity of II Peg during the years 2004-2010 to determine long- and short-term changes in the magnetic activity. We published 12 new temperature maps that showed spots distributed mainly at high and intermediate latitudes. The activity level of the star was clearly lower than during our previous study for the years 1994-2002 and we detected no clear drift of the active regions with respect to the rotation of the star. II Peg had apparently entered a state of weaker activity than during 1994-2002, and this could be related to a minimum in the star's magnetic cycle. The observations were from different wavelength regions than in paper I and some parameters had to be adjusted.

The author was collaborating in the spot modeling and analysis of the results as well as writing with Thomas Hackman and Maarit Mantere.

Paper III

Hackman, T.; Mantere, M. J.; Jetsu, L.; Ilyin, I.; Kajatkari, P.; Kochukhov, O. Lehtinen, J.; **Lindborg, M.**; Piskunov, N.; Tuominen, I.: Spot activity of II Peg, Astronomische Nachrichten, Vol.332, 859-865, 2011.

We summarized our previously published observations in Paper I and Paper II, and presented 28 Doppler imaging temperature maps using a consistent set of parameters spanning the years 1994-2010. The maps were compared with epochs of the light curve minima, derived from photometric observations. We confirmed the longitudinal drift of the major spot structure also with photometry during 1995-2003. After this there was a clear decrease in the activity level and no clear drift could be seen. These variations could be caused by a cyclic behaviour of the underlying magnetic dynamo.

The author was contributing by interpreting the Doppler images, and the observations and results from paper I were used in this article.

Paper IV

Lindborg, M.; Mantere, M. J.; Olspert, N.; Pelt, J.; Hackman, T.; Henry, G. W.; Jetsu, L.; Strassmeier, K. G.: Multiperiodicity, modulations and flip-flops in variable star light curves. II. Analysis of II Pegasus photometry during 1979-2010, Astronomy & Astrophysics, Volume 559, A97, 10p, 2013.

We wanted to further investigate from a more extensive photometric dataset whether the observed drift reported in our previous papers I and III was a persistent phenomenon, in which case it could be caused either by an azimuthal dynamo wave or be an indication that the binary system's orbital synchronization is still

incomplete. On a differentially rotating stellar surface, spot structures preferentially on a certain latitude band could also cause such a drift, the disruption of which could arise from the change of the preferred spot latitude.

We combined all collected photometric data into one single data set and analyzed it with the Carrier Fit method. We confirmed the previously published results that the spot activity had been dominated by one primary spotted region almost through the entire data set and also confirmed a persistent, nearly linear drift. We found that an alternative explanation of the drift would be a weak anti-solar (pole rotating faster than the equator) differential rotation combined with the preferred latitude of the spot structure. Later numerical simulations made by Cole *et al.* (2014) showed that the most natural explanation for this drift would after all be an azimuthal dynamo wave.

The CF analysis was done by Jaan Pelt, and analysis of the results and their influence to the activity cycles were interpreted by the author together with Maarit Mantere and Jaan Pelt. The author was responsible for the writing.

Paper V

Lindborg, M.; Hackman, T.; Mantere, M.J.; Korhonen, H.; Ilyin, I.; Kochukhov, O;Piskunov, N.: Doppler images of DI Psc during 2004-2006, Astronomy & Astrophysics, Volume 562, A139, 7p, 2014.

We studied the rapidly rotating K-giant DI Psc, that has an abnormally high lithium abundance. We published three new Doppler imaging temperature maps for the star. In July-August 2004 no clear spot structures were visible, but in July 2005 the spot coverage increased, and cool spots emerged especially at intermediate latitudes. Later on in September 2006, the spot coverage had increased and cool spots were visible at both sides of the equator.

We compared the results with earlier Doppler maps of DI Psc, and temperature maps obtained for other late-type stars with similar rotation rates, and DI Psc seemed to be in a low activity state especially during the observing season of Jul-Aug 2004. During the 2005 and 2006 observing seasons the spot activity seen in the spectral line profiles and inferred from Doppler images increased. The spot activity level of the star could be concluded to be strongly variable over time.

The spot modeling and analysis of the results were made by the author. The analysis of the publication were heavily influenced by the discussions about the dynamo theory and observational viewpoint of it with Maarit Mantere and Thomas Hackman. The author had the main responsibility of writing.

Bibliography

Arlt, R., Hollerbach, R., and Rüdiger, G. (2003). Differential rotation decay in the radiative envelopes of CP stars. *A&A*, **401**, 1087–1094.

Arlt, R., Sule, A., and Rüdiger, G. (2007). Stability of toroidal magnetic fields in the solar tachocline. *A&A*, **461**, 295–301.

Babcock, H. W. (1961). The Topology of the Sun's Magnetic Field and the 22-years Cycle. *ApJ*, **133**, 572.

Balachandran, S. C., Fekel, F. C., Henry, G. W., and Uitenbroek, H. (2000). Two K Giants with Supermeteoritic Lithium Abundances: HDE 233517 and HD 9746. *ApJ*, **542**, 978–988.

Baliunas, S. and Jastrow, R. (1990). Evidence for long-term brightness changes of solar-type stars. *Nature*, **348**, 520–523.

Baliunas, S. L., Horne, J. H., Porter, A., Duncan, D. K., Frazer, J., Lanning, H., Misch, A., Mueller, J., Noyes, R. W., Soyumer, D., Vaughan, A. H., and Woodard, L. (1985). Time-series measurements of chromospheric CA II H and K emission in cool stars and the search for differential rotation. *ApJ*, **294**, 310–325.

Baliunas, S. L., Donahue, R. A., Soon, W. H., Horne, J. H., Frazer, J., Woodard-Eklund, L., Bradford, M., Rao, L. M., Wilson, O. C., Zhang, Q., Bennett, W., Briggs, J., Carroll, S. M., Duncan, D. K., Figueroa, D., Lanning, H. H., Misch, T., Mueller, J., Noyes, R. W., Poppe, D., Porter, A. C., Robinson, C. R., Russell, J., Shelton, J. C., Soyumer, T., Vaughan, A. H., and Whitney, J. H. (1995). Chromospheric variations in main-sequence stars. *ApJ*, **438**, 269–287.

Barnes, J. R. and Collier Cameron, A. (2001). Starspot patterns on the M dwarfs HK Aqr and RE 1816 +541. *MNRAS*, **326**, 950–958.

Baryshnikova, I. and Shukurov, A. (1987). Oscillatory alpha-squared dynamo - Numerical investigation. *Astronomische Nachrichten*, **308**, 89–100.

Baumann, I., Schmitt, D., Schüssler, M., and Solanki, S. K. (2004). Evolution of the large-scale magnetic field on the solar surface: A parameter study. *A&A*, **426**, 1075–1091.

Beck, J. G. (2000). A comparison of differential rotation measurements - (Invited Review). *Sol. Phys.*, **191**, 47–70.

Berdyugina, S. V. (2002). Sunspot and starspot interiors as seen from molecular lines. *Astronomische Nachrichten*, **323**, 192–195.

Berdyugina, S. V. (2005). Starspots: A Key to the Stellar Dynamo. *Living Reviews in Solar Physics*, **2**, 5–62.

Berdyugina, S. V. and Tuominen, I. (1998). Permanent active longitudes and activity cycles on RS CVn stars. *A&A*, **336**, 25–28.

Berdyugina, S. V., Jankov, S., Ilyin, I., Tuominen, I., and Fekel, F. C. (1998a). The active RS Canum Venaticorum binary II Pegasi. I. Stellar and orbital parameters. *A&A*, **334**, 863–872.

Berdyugina, S. V., Berdyugin, A. V., Ilyin, I., and Tuominen, I. (1998b). The active RS Canum Venaticorum binary II Pegasi. II. Surface images for 1992-1996. *A&A*, **340**, 437–446.

Berdyugina, S. V., Ilyin, I., and Tuominen, I. (1999a). The active RS Canum Venaticorum binary II Pegasi. III. Chromospheric emission and flares in 1994-1996. *A&A*, **349**, 863–872.

Berdyugina, S. V., Berdyugin, A. V., Ilyin, I., and Tuominen, I. (1999b). The active RS Canum Venaticorum binary II Pegasi. IV. The SPOT activity cycle. *A&A*, **350**, 626–634.

Berdyugina, S. V., Ilyin, I., and Tuominen, I. (1999c). The long-period RS Canum Venaticorum binary IM Pegasi. I. Orbital and stellar parameters. *A&A*, **347**, 932–936.

Boyd, T. J. M. and Sanderson, J. J. (2003). *The Physics of Plasmas*. Cambridge University Press.

Brandenburg, A. (2005). The Case for a Distributed Solar Dynamo Shaped by Near-Surface Shear. *ApJ*, **625**, 539–547.

Brandenburg, A. and Subramanian, K. (2005). Astrophysical magnetic fields and nonlinear dynamo theory. *Phys. Rep.*, **417**, 1–209.

Brandenburg, A., Saar, S. H., and Turpin, C. R. (1998). Time Evolution of the Magnetic Activity Cycle Period. *ApJ*, **498**, 51–54.

Brandenburg, A., Candelaresi, S., and Chatterjee, P. (2009). Small-scale magnetic helicity losses from a mean-field dynamo. *MNRAS*, **398**, 1414–1422.

Brandenburg, A., Kemel, K., Kleeorin, N., Mitra, D., and Rogachevskii, I. (2011a). Detection of Negative Effective Magnetic Pressure Instability in Turbulence Simulations. *ApJ*, **740**, 50–54.

Brandenburg, A., Subramanian, K., Balogh, A., and Goldstein, M. L. (2011b). Scale Dependence of Magnetic Helicity in the Solar Wind. *ApJ*, **734**, 9.

Brown, S. F., Donati, J.-F., Rees, D. E., and Semel, M. (1991). Zeeman-Doppler imaging of solar-type and AP stars. IV - Maximum entropy reconstruction of 2D magnetic topologies. *A&A*, **250**, 463–474.

Brun, A. S. and Palacios, A. (2009). Numerical Simulations of a Rotating Red Giant Star. I. Three-dimensional Models of Turbulent Convection and Associated Mean Flows. *ApJ*, **702**, 1078–1097.

Budding, E. (1977). The interpretation of cyclical photometric variations in certain dwarf ME-type stars. *Ap&SS*, **48**, 207–223.

Byrne, P. B., Abdul Aziz, H., Amado, P. J., Arevalo, M. J., Avgoloupis, S., Doyle, J. G., Eibe, M. T., Elliott, K. H., Jeffries, R. D., Lanzafame, A. C., Lazaro, C., Murphy, H. M., Neff, J. E., Panov, K. P., Sarro, L. M., Seiradakis, J. H., and Spencer, R. E. (1998). The photosphere and chromosphere of the RS Canum Venaticorum star, II Pegasi. II. A multi-wavelength campaign in August/September 1992. *A&AS*, **127**, 505–519.

Carrington, R. C. (1863). *Observations of the spots on the Sun*. Williams & Norgate.

Carroll, T. A., Kopf, M., Strassmeier, K. G., Ilyin, I., and Tuominen, I. (2009). Zeeman-Doppler imaging of II Peg. *IAU Symposium*, **259**, 437–438.

Carroll, T. A., Strassmeier, K. G., Rice, J. B., and Künstler, A. (2012). The magnetic field topology of the weak-lined T Tauri star V410 Tauri. New strategies for Zeeman-Doppler imaging. *A&A*, **548**, 95–113.

Cattaneo, F. and Vainshtein, S. I. (1991). Suppression of turbulent transport by a weak magnetic field. *ApJ*, **376**, 21–24.

Chae, J. (2000). The Magnetic Helicity Sign of Filament Chirality. *ApJ*, **540**, 115–118.

Charbonneau, P. (2010). Dynamo Models of the Solar Cycle. *Living Reviews in Solar Physics*, **7**, 7–75.

Charbonnel, C. and Balachandran, S. C. (2000). The Nature of the lithium rich giants. Mixing episodes on the RGB and early-AGB. *A&A*, **359**, 563–572.

Cole, E., Käpylä, P. J., Mantere, M. J., and Brandenburg, A. (2014). An Azimuthal Dynamo Wave in Spherical Shell Convection. *ApJ*, **780**, 22–27.

Collier Cameron, A., Donati, J.-F., and Semel, M. (2002). Stellar differential rotation from direct star-spot tracking. *MNRAS*, **330**, 699–706.

Cowling, T. (1934). The magnetic field of sunspots. *MNRAS*, **94**, 39–48.

de La Reza, R. and da Silva, L. (1995). Lithium abundances in strong lithium K giant stars: LTE and non-LTE analyses. *ApJ*, **439**, 917–927.

Del Sordo, F., Guerrero, G., and Brandenburg, A. (2013). Turbulent dynamos with advective magnetic helicity flux. *MNRAS*, **429**, 1686–1694.

Démoulin, P., Mandrini, C. H., Van Driel-Gesztelyi, L., Lopez Fuentes, M. C., and Aulanier, G. (2002). The Magnetic Helicity Injected by Shearing Motions. *Sol. Phys.*, **207**, 87–110.

DeVore, C. R. (2000). Magnetic Helicity Generation by Solar Differential Rotation. *ApJ*, **539**, 944–953.

Dikpati, M. and Gilman, P. A. (2001). Flux-Transport Dynamos with α-Effect from Global Instability of Tachocline Differential Rotation: A Solution for Magnetic Parity Selection in the Sun. *ApJ*, **559**, 428–442.

Donahue, R. A., Saar, S. H., and Baliunas, S. L. (1996). A Relationship between Mean Rotation Period in Lower Main-Sequence Stars and Its Observed Range. *ApJ*, **466**, 384.

Donati, J.-F., Semel, M., and Rees, D. E. (1992). Circularly polarized spectroscopic observations of RS CVn systems. *A&A*, **265**, 669–681.

Donati, J.-F., Semel, M., Carter, B. D., Rees, D. E., and Collier Cameron, A. (1997). Spectropolarimetric observations of active stars. *MNRAS*, **291**, 658–682.

Dorren, J. D. (1987). A new formulation of the starspot model, and the consequences of starspot structure. *ApJ*, **320**, 756–767.

Doyle, J. G., Kellett, B. J., Butler, C. J., Byrne, P. B., Neff, J. E., Brown, A., Fox, D., Linsky, J. L., Bromage, G. E., Avgoloupis, S., Mavridis, L. N., Seiradakis, J. H., Mathioudakis, M., Murphy, H. M., Krzesinski, J., Pajdosz, G., Dadonas, V., Sperauskas, J., van Wyk, F., Marang, F., Olah, K., Collier Cameron, A., Antonomoulos, E., Rovithis, P., and Rovithis-Livaniou, H. (1992). Dynamic phenomena on the RS Canum Venaticorum binary Pi Pegasi in August 1989. I - Observational data. *A&AS*, **96**, 351–373.

Drake, N. A., de la Reza, R., da Silva, L., and Lambert, D. L. (2002). Rapidly Rotating Lithium-rich K Giants: The New Case of the Giant PDS 365. *AJ*, **123**, 2703–2714.

Duvall, Jr., T. L., Dziembowski, W. A., Goode, P. R., Gough, D. O., Harvey, J. W., and Leibacher, J. W. (1984). Internal rotation of the sun. *Nature*, **310**, 22–25.

Eaton, J. A. and Hall, D. S. (1979). Starspots as the cause of the intrinsic light variations in RS Canum Venaticorum type stars. *ApJ*, **227**, 907–922.

Elstner, D. and Korhonen, H. (2005). Flip-flop phenomenon: observations and theory. *Astronomische Nachrichten*, **326**, 278–282.

Gastine, T., Yadav, R. K., Morin, J., Reiners, A., and Wicht, J. (2014). From solar-like to antisolar differential rotation in cool stars. *MNRAS*, **438**, 76–80.

Gilman, P. A. (1983). Dynamically consistent nonlinear dynamos driven by convection in a rotating spherical shell. II - Dynamos with cycles and strong feedbacks. *ApJS*, **53**, 243–268.

Goncharskii, A. V., Stepanov, V. V., Kokhlova, V. L., and Yagola, A. G. (1977). Reconstruction of local line profiles from those observed in an Ap spectrum. *Soviet Astronomy Letters*, **3**, 147–149.

Goncharskii, A. V., Stepanov, V. V., Khokhlova, V. L., and Yagola, A. G. (1982). Mapping of chemical elements on the surfaces of Ap stars. I. Solution of the inverse problem of finding local profiles of spectral lines. *Soviet Ast.*, **26**, 690–696.

Gray, D. F. (2008). *The Observation and Analysis of Stellar Photospheres*. Cambridge University Press.

Gu, S.-H., Tan, H.-S., Wang, X.-B., and Shan, H.-G. (2003). Starspot activity on the RS CVn-type binary II Pegasi during 1999-2001. *A&A*, **405**, 763–768.

Guerrero, G., Smolarkiewicz, P. K., Kosovichev, A. G., and Mansour, N. N. (2013). Differential Rotation in Solar-like Stars from Global Simulations. *ApJ*, **779**, 176.

Hackman, T. (2004). *Doppler imaging and photometric time series analysis of stellar spot activity*. PHD Thesis, University of Helsinki Observatory Reports 1/2004.

Hackman, T., Mantere, M. J., Jetsu, L., Ilyin, I., Kajatkari, P., Kochukhov, O., Lehtinen, J., Lindborg, M., Piskunov, N., and Tuominen, I. (2011). Spot activity of II Peg. *Astronomische Nachrichten*, **332**, 859–865.

Hackman, T., Mantere, M. J., Lindborg, M., Ilyin, I., Kochukhov, O., Piskunov, N., and Tuominen, I. (2012). Doppler images of II Pegasi for 2004-2010. *A&A*, **538**, 126–134.

Hackman, T., Pelt, J., Mantere, M. J., Jetsu, L., Korhonen, H., Granzer, T., Kajatkari, P., Lehtinen, J., and Strassmeier, K. G. (2013). Flip-flops of Comae Berenices. *A&A*, **553**, 40–53.

Hale, G. E. (1908). On the Probable Existence of a Magnetic Field in Sun-Spots. *ApJ*, **28**, 315–348.

Hale, G. E., Ellerman, F., Nicholson, S. B., and Joy, A. H. (1919). The Magnetic Polarity of Sun-Spots. *ApJ*, **49**, 153–186.

Hall, D. S. (1972). A T Tauri-Like Star in the Eclipsing Binary RS Canum Venaticorum. *PASP*, **84**, 323.

Hall, D. S. (1976). The RS CVn Binaries and Binaries with Similar Properties. In W. S. Fitch, editor, *IAU Colloq. 29: Multiple Periodic Variable Stars*, volume 60 of *Astrophysics and Space Science Library*, page 287.

Hall, D. S. (1991). A connection between long-term luminosity variations and orbital period changes in chromospherically active binaries. *ApJ*, **380**, 85–87.

Hatzes, A. P. (1993). The spot Distribution on II Peg in 1992. In *American Astronomical Society Meeting Abstracts #182*, volume 25 of *Bulletin of the American Astronomical Society*, page 874.

Hatzes, A. P., Vogt, S. S., Ramseyer, T. F., and Misch, A. (1996). The Inclination Dependence of the Mean Spectral Line Shapes of RS CVn Stars: Further Evidence for Polar Spots. *ApJ*, **469**, 808–818.

Henry, G. W., Eaton, J. A., Hamer, J., and Hall, D. S. (1995). Starspot evolution, differential rotation, and magnetic cycles in the chromospherically active binaries λ andromedae, σ Geminorum, II Pegasi, and V711 Tauri. *ApJS*, **97**, 513–549.

Holzwarth, V. and Schüssler, M. (2003). Dynamics of magnetic flux tubes in close binary stars. II. Nonlinear evolution and surface distributions. *A&A*, **405**, 303–311.

Howe, R. (2009). Solar interior rotation and its variation. *Living Reviews in Solar Physics*, **6**(1).

Hubbard, A. and Brandenburg, A. (2011). Magnetic Helicity Flux in the Presence of Shear. *ApJ*, **727**, 11.

Hubbard, A. and Brandenburg, A. (2012). Catastrophic Quenching in $\alpha\Omega$ Dynamos Revisited. *ApJ*, **748**, 51.

Iben, Jr., I. (1968). Low-Mass Red Giants. *ApJ*, **154**, 581–597.

Jetsu, L. and Pelt, J. (1999). Three stage period analysis and complementary methods. *A&AS*, **139**, 629–643.

Jetsu, L., Pelt, J., and Tuominen, I. (1993). Spot and flare activity of FK Comae Berenices: Long-term photometry. *A&A*, **278**, 449–462.

Kajatkari, P., Hackman, T., Jetsu, L., Lehtinen, J., and Henry, G. W. (2014). Spot activity of the RS Canum Venaticorum star σ Geminorum. *A&A*, **562**, 107–117.

Käpylä, P. J. (2011). On global solar dynamo simulations. *Astronomische Nachrichten*, **332**, 43.

Käpylä, P. J., Korpi, M. J., and Tuominen, I. (2004). Local models of stellar convection:. Reynolds stresses and turbulent heat transport. *A&A*, **422**, 793–816.

Käpylä, P. J., Korpi, M. J., Ossendrijver, M., and Tuominen, I. (2005). Estimates of the Strouhal number from numerical models of convection. *Astronomische Nachrichten*, **326**, 186–189.

Käpylä, P. J., Korpi, M. J., Ossendrijver, M., and Stix, M. (2006). Magnetoconvection and dynamo coefficients. III. α-effect and magnetic pumping in the rapid rotation regime. *A&A*, **455**, 401–412.

Käpylä, P. J., Korpi, M. J., and Brandenburg, A. (2008). Large-scale dynamos in turbulent convection with shear. *A&A*, **491**, 353–362.

Käpylä, P. J., Korpi, M. J., and Brandenburg, A. (2009). Alpha effect and turbulent diffusion from convection. *A&A*, **500**, 633–646.

Käpylä, P. J., Mantere, M. J., and Brandenburg, A. (2011a). Effects of stratification in spherical shell convection. *Astronomische Nachrichten*, **332**, 883–890.

Käpylä, P. J., Mantere, M. J., Guerrero, G., Brandenburg, A., and Chatterjee, P. (2011b). Reynolds stress and heat flux in spherical shell convection. *A&A*, **531**, 162–179.

Käpylä, P. J., Mantere, M. J., and Hackman, T. (2011c). Starspots due to Large-scale Vortices in Rotating Turbulent Convection. *ApJ*, **742**, 34–42.

Käpylä, P. J., Mantere, M. J., and Brandenburg, A. (2012). Cyclic Magnetic Activity due to Turbulent Convection in Spherical Wedge Geometry. *ApJ*, **755**, 22–27.

Käpylä, P. J., Mantere, M. J., and Brandenburg, A. (2013). Oscillatory large-scale dynamos from Cartesian convection simulations. *Geophysical and Astrophysical Fluid Dynamics*, **107**, 244–257.

Karak, B. B., Rheinhardt, M., Brandenburg, A., Käpylä, P. J., and Käpylä, M. J. (2014). Quenching and Anisotropy of Hydromagnetic Turbulent Transport. *ApJ*, **795**, 16.

Kővári, Z., Korhonen, H., Strassmeier, K. G., Weber, M., Kriskovics, L., and Savanov, I. (2013). Doppler imaging of stellar surface structure. XXIV. The lithium-rich single K-giants DP Canum Venaticorum and DI Piscium. *A&A*, **551**, 2–13.

Kitchatinov, L. L. and Rüdiger, G. (1999). Differential rotation models for late-type dwarfs and giants. *A&A*, **344**, 911–917.

Kitchatinov, L. L. and Rüdiger, G. (2004). Anti-solar differential rotation. *Astronomische Nachrichten*, **325**, 496–500.

Kitchatinov, L. L. and Rüdiger, G. (2006). Magnetic field confinement by meridional flow and the solar tachocline. *A&A*, **453**, 329–333.

Kochukhov, O., Makaganiuk, V., and Piskunov, N. (2010). Least-squares deconvolution of the stellar intensity and polarization spectra. *A&A*, **524**, 5–19.

Kochukhov, O., Mantere, M. J., Hackman, T., and Ilyin, I. (2013). Magnetic field topology of the RS CVn star II Pegasi. *A&A*, **550**, 84–103.

Kopf, M. (2009). *Zeeman-Doppler Imaging of active late-type stars*. PHD Thesis.

Krause, F. and Rädler, K.-H. (1980). *Mean-field magnetohydrodynamics and dynamo theory*. Wiley.

Kriskovics, L., Kővári, Z., Vida, K., and Oláh, K. (2013). Activity on a Li-rich giant: DI Psc revisited. *ArXiv e-prints*.

Küker, M. and Stix, M. (2001). Differential rotation of the present and the pre-main-sequence Sun. *A&A*, **366**, 668–675.

Kumar, Y. B., Reddy, B. E., and Lambert, D. L. (2011). Origin of Lithium Enrichment in K Giants. *ApJ*, **730**, 12–17.

Kupka, F., Piskunov, N., Ryabchikova, T. A., Stempels, H. C., and Weiss, W. W. (1999). VALD-2: Progress of the Vienna Atomic Line Data Base. *A&AS*, **138**, 119–133.

Leighton, R. B. (1969). A Magneto-Kinematic Model of the Solar Cycle. *ApJ*, **156**, 1.

Lindborg, M., Korpi, M. J., Hackman, T., Tuominen, I., Ilyin, I., and Piskunov, N. (2011). Doppler images of the RS CVn binary II Pegasi during the years 1994-2002. *A&A*, **526**, 44–51.

Lindborg, M., Mantere, M. J., Olspert, N., Pelt, J., Hackman, T., Henry, G. W., Jetsu, L., and Strassmeier, K. G. (2013). Multiperiodicity, modulations and flip-flops in variable star light curves. II. Analysis of II Pegasus photometry during 1979-2010. *A&A*, **559**, 97–107.

Lindborg, M., Hackman, T., Mantere, M. J., Korhonen, H., Ilyin, I., Kochukhov, O., and Piskunov, N. (2014). Doppler images of DI Piscium during 2004-2006. *A&A*, **562**, 139–146.

Lockwood, G. W., Skiff, B. A., Henry, G. W., Henry, S., Radick, R. R., Baliunas, S. L., Donahue, R. A., and Soon, W. (2007). Patterns of Photometric and Chromospheric Variation among Sun-like Stars: A 20 Year Perspective. *ApJS*, **171**, 260–303.

Mantere, M. J., Käpylä, P. J., and Hackman, T. (2011). Dependence of the large-scale vortex instability on latitude, stratification, and domain size. *Astronomische Nachrichten*, **332**, 876–882.

Mathur, S., García, R. A., Ballot, J., Ceillier, T., Salabert, D., Metcalfe, T. S., Régulo, C., Jiménez, A., and Bloemen, S. (2014). Magnetic activity of F stars observed by Kepler. *A&A*, **562**, 124–148.

Matt, S. P., Do Cao, O., Brown, B. P., and Brun, A. S. (2011). Convection and differential rotation properties of G and K stars computed with the ASH code. *Astronomische Nachrichten*, **332**, 897.

Melo, C. H. F., de Laverny, P., Santos, N. C., Israelian, G., Randich, S., Do Nascimento, Jr., J. D., and de Medeiros, J. R. (2005). On the nature of lithium-rich giant stars. Constraints from beryllium abundances. *A&A*, **439**, 227–235.

Messina, S., Guinan, E. F., Lanza, A. F., and Ambruster, C. (1999). Activity cycle and surface differential rotation of the single Pleiades star HD 82443 (DX Leo). *A&A*, **347**, 249–257.

Miesch, M. S., Brun, A. S., and Toomre, J. (2006). Solar Differential Rotation Influenced by Latitudinal Entropy Variations in the Tachocline. *ApJ*, **641**, 618–625.

Miesch, M. S., Brown, B. P., Browning, M. K., Brun, A. S., and Toomre, J. (2011). Magnetic Cycles and Meridional Circulation in Global Models of Solar Convection. In N. H. Brummell, A. S. Brun, M. S. Miesch, and Y. Ponty, editors, *IAU Symposium*, volume 271 of *IAU Symposium*, pages 261–269.

Mitra, D., Tavakol, R., Käpylä, P. J., and Brandenburg, A. (2010). Oscillatory Migrating Magnetic Fields in Helical Turbulence in Spherical Domains. *ApJ*, **719**, 1–4.

Moss, D., Tuominen, I., and Brandenburg, A. (1991). Nonlinear nonaxisymmetric dynamo models for cool stars. *A&A*, **245**, 129–135.

Oláh, K. and Strassmeier, K. G. (2002). Starspot cycles from long-term photometry. *Astronomische Nachrichten*, **323**, 361–366.

Oláh, K., Kolláth, Z., Granzer, T., Strassmeier, K. G., Lanza, A. F., Järvinen, S., Korhonen, H., Baliunas, S. L., Soon, W., Messina, S., and Cutispoto, G. (2009). Multiple and changing cycles of active stars. II. Results. *A&A*, **501**, 703–713.

Parker, E. N. (1955). Hydromagnetic Dynamo Models. *ApJ*, **122**, 293–315.

Pelt, J., Korpi, M. J., and Tuominen, I. (2010). Solar active regions: a nonparametric statistical analysis. *A&A*, **513**, 48–55.

Pelt, J., Olspert, N., Mantere, M. J., and Tuominen, I. (2011). Multiperiodicity, modulations and flip-flops in variable star light curves. I. Carrier fit method. *A&A*, **535**, 23–35.

Petit, P., Donati, J.-F., Wade, G. A., Landstreet, J. D., Bagnulo, S., Lüftinger, T., Sigut, T. A. A., Shorlin, S. L. S., Strasser, S., Aurière, M., and Oliveira, J. M. (2004). Magnetic topology and surface differential rotation on the K1 subgiant of the RS CVn system HR 1099. *MNRAS*, **348**, 1175–1190.

Petit, P., Dintrans, B., Morgenthaler, A., Van Grootel, V., Morin, J., Lanoux, J., Aurière, M., and Konstantinova-Antova, R. (2009). A polarity reversal in the large-scale magnetic field of the rapidly rotating sun HD 190771. *A&A*, **508**, 9–12.

Pipin, V. V. and Kosovichev, A. G. (2013). The Mean-field Solar Dynamo with a Double Cell Meridional Circulation Pattern. *ApJ*, **776**, 36–45.

Pipin, V. V., Moss, D., Sokoloff, D., and Hoeksema, J. T. (2014). Reversals of the solar magnetic dipole in the light of observational data and simple dynamo models. *A&A*, **567**, A90.

Piskunov, N. E. (1991). The Art of Surface Imaging. In I. Tuominen, D. Moss, and G. Rüdiger, editors, *IAU Colloq. 130: The Sun and Cool Stars. Activity, Magnetism, Dynamos*, volume 380 of *Lecture Notes in Physics, Berlin Springer Verlag*, page 309.

Piskunov, N. E., Tuominen, I., and Vilhu, O. (1990). Surface imaging of late-type stars. *A&A*, **230**, 363–370.

Radick, R. R., Lockwood, G. W., and Baliunas, S. L. (1990). Stellar activity and brightness variations - A glimpse at the sun's history. *Science*, **247**, 39–44.

Reddy, B. E. and Lambert, D. L. (2005). Three Li-rich K Giants: IRAS 12327-6523, 13539-4153, and 17596-3952. *AJ*, **129**, 2831–2835.

Reinhold, T., Reiners, A., and Basri, G. (2013). Rotation and differential rotation of active Kepler stars. *A&A*, **560**, A4.

Rice, J. B. (2002). Doppler imaging of stellar surfaces - techniques and issues. *Astronomische Nachrichten*, **323**, 220–235.

Rice, J. B. and Strassmeier, K. G. (2000). Doppler imaging from artificial data. Testing the temperature inversion from spectral-line profiles. *A&AS*, **147**, 151–168.

Rodonò, M. (2000). Magnetic activity phenomena on stars: from the photosphere up to the transition region layers. In R. Pallavicini, G. Micela, and S. Sciortino, editors, *Stellar Clusters and Associations: Convection, Rotation, and Dynamos*, volume 198 of *ASPCS*, pages 391–401.

Rodonò, M., Cutispoto, G., Pazzani, V., Catalano, S., Byrne, P. B., Doyle, J. G., Butler, C. J., Andrews, A. D., Blanco, C., Marilli, E., Linsky, J. L., Scaltriti, F., Busso, M., Cellino, A., Hopkins, J. L., Okazaki, A., Hayashi, S. S., Zeilik, M., Helston, R., Henson, G., Smith, P., and Simon, T. (1986). Rotational modulation and flares on RS CVn and BY Dra-type stars. I - Photometry and spot models for BY Dra, AU Mic, AR Lac, II Peg and V 711 Tau (= HR 1099). *A&A*, **165**, 135–156.

Roettenbacher, R. M., Harmon, R. O., Vutisalchavakul, N., and Henry, G. W. (2011). A Study of Differential Rotation on II Pegasi via Photometric Starspot Imaging. *AJ*, **141**, 138–159.

Rosén, L. and Kochukhov, O. (2012). How reliable is Zeeman Doppler imaging without simultaneous temperature reconstruction? *A&A*, **548**, 8–20.

Rosén, L., Kochukhov, O., and Wade, G. A. (2013). Strong variable linear polarization in the cool active star II Peg. *MNRAS*, **436**, 10–14.

Rüdiger, G. (1989). *Differential rotation and stellar convection. Sun and the solar stars*. Berlin Akademie Verlag.

Rüdiger, G. and Küker, M. (2002). Meridional flow and differential rotation by gravity darkening in fast rotating solar-type stars. *A&A*, **385**, 308–312.

Rüdiger, G., Elstner, D., and Ossendrijver, M. (2003). Do spherical α^2-dynamos oscillate? *A&A*, **406**, 15–21.

Saar, S. H. and Brandenburg, A. (1999). Time Evolution of the Magnetic Activity Cycle Period. II. Results for an Expanded Stellar Sample. *ApJ*, **524**, 295–310.

Schüssler, M. and Ferriz-Mas, A. (2003). Magnetic flux tubes and the dynamo problem. *Advances in Nonlinear Dynamics*, pages 123–146.

Schüssler, M. and Solanki, S. K. (1992). Why rapid rotators have polar spots. *A&A*, **264**, 13–16.

Schwabe, M. (1844). Sonnenbeobachtungen im Jahre 1843. Von Herrn Hofrath Schwabe in Dessau. *Astronomische Nachrichten*, **21**, 233–234.

Schwartz, D. A., Garcia, M., Ralph, E., Doxsey, R. E., Johnston, M. D., Lawrence, A., McHardy, I. M., and Pye, J. P. (1981). Identification of the fast, high galactic latitude X-ray transient A 0000 + 28 with the RS CVn system HD 224085. *MNRAS*, **196**, 95–100.

Schwarzenberg-Czerny, A. (2003). An astronomer's guide to period searching. In C. Sterken, editor, *Interplay of Periodic, Cyclic and Stochastic Variability in Selected Areas of the H-R Diagram*, volume 292 of *ASPCS*, pages 383–391.

Semel, M. (1989). Zeeman-Doppler imaging of active stars. I - Basic principles. *A&A*, **225**, 456–466.

Siwak, M., Rucinski, S. M., Matthews, J. M., Kuschnig, R., Guenther, D. B., Moffat, A. F. J., Sasselov, D., and Weiss, W. W. (2010). Analysis of the MOST light curve of the heavily spotted K2IV component of the single-line spectroscopic binary II Pegasi. *MNRAS*, **408**, 314–321.

Snodgrass, H. B. and Ulrich, R. K. (1990). Rotation of Doppler features in the solar photosphere. *ApJ*, **351**, 309–316.

Solanki, S. K., Usoskin, I. G., Kromer, B., Schüssler, M., and Beer, J. (2004). Unusual activity of the Sun during recent decades compared to the previous 11,000 years. *Nature*, **431**, 1084–1087.

Spruit, H. C. (1981). Equations for thin flux tubes in ideal MHD. *A&A*, **102**, 129–133.

Steenbeck, M., Krause, F., and Rädler, K.-H. (1966). Berechnung der mittleren Lorentz-Feldstärke $v \times b$ für ein elektrisch leitendes Medium in turbulenter, durch Coriolis-Kräfte beeinflußter Bewegung. *Zeitschrift Naturforschung Teil A*, **21**, 369.

Strassmeier, K., Washuettl, A., Granzer, T., Scheck, M., and Weber, M. (2000). The Vienna-KPNO search for Doppler-imaging candidate stars. I. A catalog of stellar-activity indicators for 1058 late-type Hipparcos stars. *A&AS*, **142**, 275–311.

Strassmeier, K. G. (1990). Photometric and spectroscopic modeling of starspots on the RS Canum Venaticorum binary HD 26337. *ApJ*, **348**, 682–699.

Strassmeier, K. G. (1999). Doppler imaging of stellar surface structure. XI. The super starspots on the K0 giant HD 12545: larger than the entire Sun. *A&A*, **347**, 225–234.

Strassmeier, K. G. (2009). Starspots. *A&A Rev.*, **17**, 251–308.

Strassmeier, K. G. and Bopp, B. W. (1992). Time-series photometric spot modeling. I - Parameter study and application to HD 17433 = VY Arietis. *A&A*, **259**, 183–197.

Strassmeier, K. G., Pichler, T., Weber, M., and Granzer, T. (2003). Doppler imaging of stellar surface structure. XXI. The rapidly-rotating solar-type star HD 171488 = V889 Hercules. *A&A*, **411**, 595–604.

Tschäpe, R. and Rüdiger, G. (2001). Rotation-induced lithium depletion of solartype stars in open stellar clusters. *A&A*, **377**, 84–89.

Tuominen, I., Berdyugina, S. V., and Korpi, M. J. (2002). Starspot cycles from Doppler imaging and photometric time series as nonlinear dynamo. *Astronomische Nachrichten*, **323**, 367–370.

Usoskin, I. G., Berdyugina, S. V., and Poutanen, J. (2005). Preferred sunspot longitudes: non-axisymmetry and differential rotation. *A&A*, **441**, 347–352.

van Leeuwen, F. (2007). Validation of the new Hipparcos reduction. *A&A*, **474**, 653–664.

Vaughan, A. H. and Preston, G. W. (1980). A survey of chromospheric CA II H and K emission in field stars of the solar neighborhood. *PASP*, **92**, 385–391.

Vishniac, E. T. and Cho, J. (2001). Magnetic Helicity Conservation and Astrophysical Dynamos. *ApJ*, **550**, 752–760.

Vogt, S. S. (1981a). A method for unambiguous determination of starspot temperatures and areas - Application to II Pegasi, BY Draconis, and HD 209813. *ApJ*, **250**, 327–340.

Vogt, S. S. (1981b). A spectroscopic, photometric, and magnetic study of the starspot on II Pegasi. *ApJ*, **247**, 975–983.

Vogt, S. S., Penrod, G. D., and Hatzes, A. P. (1987). Doppler images of rotating stars using maximum entropy image reconstruction. *ApJ*, **321**, 496–515.

Warnecke, J., Käpylä, P. J., Mantere, M. J., and Brandenburg, A. (2013). Spoke-like Differential Rotation in a Convective Dynamo with a Coronal Envelope. *ApJ*, **778**, 141–156.

Weber, M., Strassmeier, K. G., and Washuettl, A. (2005). Indications for anti-solar differential rotation of giant stars. *Astronomische Nachrichten*, **326**, 287–291.

Wilson, O. C. (1978). Chromospheric variations in main-sequence stars. *ApJ*, **226**, 379–396.

Xiang, Y., Gu, S.-h., Cameron, A. C., and Barnes, J. R. (2014). Distribution and evolution of starspots on the RS CVn binary II Pegasi in 2004. *MNRAS*, **438**, 2307–2316.

Yoshimura, H. (1975). Solar-cycle dynamo wave propagation. *ApJ*, **201**, 740–748.

Zhao, J., Bogart, R. S., Kosovichev, A. G., Duvall, Jr., T. L., and Hartlep, T. (2013). Detection of Equatorward Meridional Flow and Evidence of Double-cell Meridional Circulation inside the Sun. *ApJ*, **774**, 29–35.